In presenting the dissertation as a partial fulfillment of the requirements for an advanced degree from the Georgia Institute of Technology, I agree that the Library of the Institute shall make it available for inspection and circulation in accordance with its regulations governing materials of this type. I agree that permission to copy from, or to publish from, this dissertation may be granted by the professor under whose direction it was written, or, in his absence, by the Dean of the Graduate Division when such copying or publication is solely for scholarly purposes and does not involve potential financial gain. It is understood that any copying from, or publication of, this dissertation which involves potential financial gain will not be allowed without written permission.

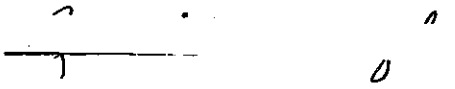

3/17/65
b

CONVERSION ELECTRON PARTICLE PARAMETER VALUES FROM DIRECTIONAL CORRELATIONS IN Pb^{207} AND Cs^{133}

A THESIS

Presented to

The Faculty of the Graduate Division

by

Russell McDill Brengelman

In Partial Fulfillment

of the Requirements for the Degree

Doctor of Philosophy in the School of Physics

Georgia Institute of Technology

September, 1967

CONVERSION ELECTRON PARTICLE PARAMETER VALUES FROM DIRECTIONAL CORRELATIONS IN Pb^{207} AND Cs^{133}

Approved:

Chairman

Date Approved by Chairman: August 25, 1967

ACKNOWLEDGMENTS

The author wishes to express his deep appreciation to Dr. E. T. Patronis, Jr. for his personal guidance and assistance during this investigation. He suggested the topic for this research and continued to give invaluable suggestions throughout the course of the investigation. The author also wishes to thank Professors C. H. Braden, L. D. Wyly, Jr., and N. S. Kendrick for their willing assistance and guidance.

The author is indebted to the National Aeronautics and Space Administration which provided an institutional grant, NsG-657, for the support of this research.

Finally, the author wishes to acknowledge the unquestioning love and support of his wife during this endeavor.

TABLE OF CONTENTS

TABLE OF CONTENTS (Concluded)

LIST OF TABLES

LIST OF ILLUSTRATIONS

SUMMARY

The decay schemes of both Pb^{207} and Cs^{133} have been extensively investigated and are well established. The present research has been a study of internal conversion processes in Pb^{207} and Cs^{133}. The specific objective has been to obtain experimental L shell conversion electron particle parameters from directional correlation measurements on the 1064 keV (M4)-570 keV (E2) cascade in Pb^{207} and the 356 keV (E2)-81 keV (M1) cascade in Cs^{133}. Comparison of these experimental parameters with the theory has been facilitated by the recent publication of tables of theoretically computed "structureless" L shell particle parameters.

The experimental arrangement for electron-gamma directional correlations consisted of a fixed electron detector and 3X3 inch NaI(Tl) gamma scintillation detectors which could be rotated about the radioactive source. Separate directional correlation measurements for electrons converted from different atomic shells were made feasible by the use of a lithium ion drift electron detector which was cooled to the temperature of dry ice. Fast-slow coincidence circuitry, which included a 400 channel pulse height analyzer, was employed in the analysis of signals from the radiation detectors.

The particle parameter, b_2, is conventionally defined as

$$b_2 = A_2(e\gamma)/A_2(\gamma\gamma) \quad ,$$

where $A_2(e\gamma)$ and $A_2(\gamma\gamma)$ denote the expansion coefficients for electron-gamma and gamma-gamma directional correlations. The coefficient for the 1064 keV gamma-570 keV gamma correlation employed in determining the particle parameters for Pb^{207} was a mean value obtained from measurements reported in the literature. The A_2 coefficient for the 356 keV gamma-81 keV gamma correlation in Cs^{133} has been remeasured in the present study.

The K-, L-, and M-shell parameters have been obtained for the 1064-keV and 570-keV transitions in Pb^{207}. In comparing experiment and theory, the results are presented in the form of a ratio of parameters, $b_2(K)/b_2(L)$ as follows:

	b_2 Experiment	Theory	Particle Parameter Ratios	Experiment	Theory
$b_2(1064K)$	1.00(3)	1.049	$b_2(K)/b_2(L)$	0.94(6)	1.020
$b_2(1064L)$	1.06(6)	1.028	$b_2(L)/b_2(M)$	1.08(11)	
$b_2(1064M)$	0.98(9)		$b_2(K)/b_2(L)$	1.07(6)	1.102
$b_2(570K)$	1.22(4)	1.204	$b_2(L)/b_2(M)$	0.95(11)	
$b_2(570L)$	1.14(5)	1.093			
$b_2(570M)$	1.20(13)				

The errors listed in the table are probable errors.

With the exception of $b_2(570L)$, the theoretical parameters obtained from the literature were calculated on the basis of the point nucleus (unscreened) model. The parameter $b_2(570L)$ was obtained by interpolation from the tables of Listengarten and Miranda which are based on a model which accounts for screening and the static effects of finite

nuclear size. No theoretical M-shell parameters have been published.

Although the L parameter is somewhat high, the experimental K- and L-particle parameters for the 570-keV transition are in substantial agreement with the theory.

The error in the ratio of experimental K and L parameters for the 1064-keV transition has been estimated conservatively. It is believed that this ratio is indeed less than unity, and is therefore in disagreement with the theoretical ratio. If this small discrepancy can be taken seriously it could indicate a small E5 admixture in the predominantly M4 transition or that screening and nuclear size effects must be accounted for in computing the L-shell parameters.

In the correlation measurements in Cs^{133}, L and M shell conversion electrons of the 356-keV transition were unresolved. The K and L+M shell particle parameters obtained for this transition are as follows:

Particle Parameters			
Experiment		Theory	
$b_2(356K)$	1.42(17)	$b_2(356K)$	1.63
$b_2(356L+M)$	1.27(24)	$b_2(356L)$	1.41

Particle Parameter Ratios			
Experiment		Theory	
$\frac{b_2(356K)}{b_2(356L+M)}$	1.12(25)	$\frac{b_2(356K)}{b_2(356L)}$	1.16

The disagreement between the experimental and theoretical parameters may be statistical in origin, but the possibility that the lower experimental values are the result of electron scattering in the source cannot be ruled out. Within the rather large error limits associated with this measurement, the ratio of the K and L+M parameters, which is less sensitive to scattering, is in agreement with the theoretical ratio for a pure E2 transition.

CHAPTER I

INTRODUCTION

The internal conversion process is one of three principal electromagnetic processes by which radioactive atoms may de-excite. The other two are gamma-ray emission and internal pair creation. Gamma emission and internal conversion are more probable modes of decay than that of internal pair creation. The latter occurs only when nuclear transition energies are above 1.02 MeV (1). During gamma emission, the recoil energy of the nucleus is negligible in comparison to the energy of the emitted gamma ray. Therefore during this process the nucleus emits a quantum of the electromagnetic field, i.e., a gamma ray, whose energy is approximately equal to the nuclear transition energy. Internal conversion is an independent process in which the excited nucleus transfers its energy through the electromagnetic field to an orbital electron. The electron is ejected from the atom with kinetic energy equal to the nuclear transition energy minus the electron's atomic binding energy. Once again, the recoil energy of the nucleus has been neglected.

During these nuclear processes, the emitted radiations are the only quantities which can be experimentally observed. Devices for the detection of these radiations have become steadily more diverse and refined. In most devices the radiation striking the detector generates a signal whose amplitude is proportional to the kinetic energy of the radiation. Thus the process of detection usually yields the energy of

the nuclear transition.

Nuclear transitions of all types, those involving the weak and strong interactions, as well as the electromagnetic processes, frequently occur in cascade. In many instances the radiations emitted during successive transitions follow one another in such rapid succession that, for measurement purposes, they are considered to be coincident. By using additional detectors and observing the radiations simultaneously, one can obtain additional information about these nuclear transition processes. The research described in this thesis was an experimental study of the internal conversion process using a measurement of this type. The directional correlation measurements consisted of the simultaneous observation of the directions of emission of successive conversion electrons and gamma rays.

The Concept of a Directional Correlation

For a single nucleus in a sample of radioactive material, the probability of emission of a particle or quantum by the nucleus depends in general on the angle between the nuclear spin axis and the direction of emission of the nuclear radiation (2). The radiation pattern from the sample as a whole will be isotropic in the laboratory coordinate system. This occurs because the spin axes of the nuclei are oriented at random throughout the sample. The radiation pattern will exhibit a directional dependence in the laboratory system only if an ensemble of nuclei whose spins are not randomly oriented can be selected.

A directional correlation measurement is one method of selecting such an ensemble experimentally. It is based on the following observations: (a) nuclear transitions often occur in rapid succession with the

lifetime of the intermediate state of the nucleus being of the order of 10^{-11} second or less, (b) the orientation of the spin of the nucleus will usually be maintained while the nucleus is in this intermediate state, and (c) angular momentum is conserved between the nucleus and the emitted radiations.

By experimentally observing the direction of emission of the first radiation in the laboratory system, one effectively selects an ensemble of nuclei in which the intermediate state spins are not randomly oriented. They are, in fact, correlated to the observed direction of emission. Since angular momentum is conserved during both transitions, the direction of emission of the second radiation will be correlated to the direction of emission of the first. If the lifetime of the intermediate nuclear state is longer than about 10^{-11} second, one must consider the possibility that the nuclear spin may be perturbed by extranuclear fields (3). The second radiation is experimentally identified as having been emitted from the same nucleus as the first radiation, and thus from the selected ensemble, by requiring a time coincidence of the electrical signals obtained from the two radiation detectors. The accuracy of this determination will be limited by the resolving time of the electronic coincidence circuit.

The radiation detectors are arranged in a horizontal plane so that their axes intersect at the radioactive source to form an angle θ. By rotating one of the detectors about a vertical axis through the source to vary the angle θ, the directional dependence of the pattern of coincident radiations can be recorded. The coincidence counting rate of the two detectors is proportional to the probability that the

successive radiations will be emitted with an angle θ between their directions of propagation.

The directional correlation is most conveniently described by mathematically expressing the probability that the two radiations will be emitted at an angle θ as a finite series of even Legendre polynomials (2),

$$w(\theta) = a_o + a_2 P_2(\cos\theta) + a_4 P_4(\cos\theta) + \ldots \quad . \qquad \text{(I-1)}$$

The number of terms in the series as well as each expansion coefficient will be a function of the angular momenta carried away by the radiations and the spins of the three nuclear states coupled by the transitions. In addition to their dependence on the angular momenta, the expansion coefficients will depend on the types of radiations emitted. The correlation function is usually written in normalized form by dividing Equation (I-1) by a_o,

$$W(\theta) = 1 + A_2 P_2(\cos\theta) + A_4 P_4(\cos\theta) \quad , \qquad \text{(I-2)}$$

where $A_2 = a_2/a_o$ and $A_4 = a_4/a_o$. The relative magnitudes of the coefficients usually decrease rapidly and experimental measurements will generally allow a determination of only the A_2 and A_4 coefficients. Therefore higher order terms, if present, have been neglected in writing Equation (I-2). The pertinent results of the theoretical development of this equation are outlined in Appendix A.

Historical Development

Because of the importance of electromagnetic transitions by nuclei, the first theoretical study of directional correlations involved successive gamma rays. This study was made by Hamilton in 1940, and the results were restricted to the emission of pure multipole radiations (4).

In 1946 Goertzel studied the influence of extranuclear fields on the orientation of the spin of the nucleus while it is in the intermediate state. The first successful experimental measurements of a gamma-gamma directional correlation were carried out by Brady and Deutsch in 1947 using Geiger counters to detect the radiations (5). The following year Brady, Metzger, and Deutsch introduced the use of scintillation counters in such measurements (6), (7). This new radiation detector represented a major advance in experimental technique. It provided better counting efficiency, speed, and energy resolution than the Geiger counter.

In 1949 Ling and Falkoff extended the theory to include gamma emissions in which mixtures of multipoles are present in the transition (8). This same year Gardner treated the theory of directional correlations between internal conversion electrons (9). Besides its relevance to the present investigation, Gardner's work is of importance because he introduced simplified mathematical procedures based on the algebra developed by Racah (10). The extension to beta-gamma directional correlations was made by Falkoff and Uhlenbeck in 1950 (11). Reviews of the general theory of directional correlations of nuclear radiations have been published by Blatt and Biedenharn (12), Biedenharn and Rose (13), and Coester and Jauch (14).

The relativistically formulated theory of conversion electron directional correlations was developed by Rose, Biedenharn, and Arfken (15). In 1955, Church and Weneser found that penetration of the orbital electron into the nuclear volume may in some cases measurably affect the conversion process. Penetration effects have been detected in retarded E1 and M1 transitions (16) as well as E2 transitions occurring in certain heavy and deformed nuclei (17). Although their contribution to the conversion process is generally small, penetration matrix elements are of considerable interest because they depend on nuclear structure. Corrections for this effect were incorporated into the theory of electron correlations by Church and Weneser (16) and by Green and Rose (18).

During the 1950's experimental development centered on fast electronic coincidence circuits (19) and on multichannel analyzers (20) for the timing and energy analyses of detected coincident radiations.

Within the past five years, the use of solid state radiation detectors has emerged as one of the more important advances in experimental technique (21). In studies which demand high energy resolution, this type of detector has supplanted the scintillation detector.

The use of a lithium drift detector with sufficient energy resolution to resolve electrons converted from different atomic shells has made the present investigation feasible.

Directional Correlations Involving Gamma Rays and Conversion Electrons

Gamma-gamma directional correlations will allow the determination of the spins of the nuclear states and the angular momenta of the emitted

gamma rays. In addition to these properties, directional correlations involving the conversion electrons of these transitions will depend on the relative parities of the nuclear states and the matrix elements of the conversion transition.

In early experimental studies, using scintillation counters for electron detection, electrons converted from different atomic shells were unresolved. Directional correlation theory treating only conversion from the K shell was applied in the data analysis to determine the spins and parities of the excited nuclear states (22). As experimental and theoretical studies have been refined and extended, correlation measurements are being applied to the study of the details of the internal conversion process. This information is obtained by a careful determination of the A_2 and A_4 expansion coefficients of the directional correlation function which depend on the conversion matrix elements.

In electron-gamma directional correlations in which the converted transition is a pure multipole transition, the correlation function is expressed as follows:

$$W_{e\gamma}(\theta) = 1 + A_2(e\gamma)P_2(\cos\theta) + A_4(e\gamma)P_4(\cos\theta) \quad . \qquad (I\text{-}3)$$

For the case of the gamma-electron correlation the expansion coefficients are denoted by $A_2(\gamma e)$ and $A_4(\gamma e)$.

Conversion Electron Particle Parameters

Internal conversion is a second order process which competes with gamma-ray emission, and the results of internal conversion studies are often compared directly to those involving gamma emission. For example,

the internal conversion coefficient is defined as the ratio of the number of conversion electrons to the number of gamma rays emitted per unit time in a nuclear transition. In conversion electron directional correlation studies, the correlation of the competing gamma-gamma transition cascade is used as the reference for comparison.

The expansion coefficients of the gamma-gamma directional correlation function,

$$W_{\gamma\gamma}(\theta) = 1 + A_2(\gamma\gamma)P_2(\cos\theta) + A_4(\gamma\gamma)P_4(\cos\theta) \quad , \qquad \text{(I-4)}$$

and those of the electron-gamma correlation are compared by defining a conversion electron particle parameter, b_ν, as follows (15):

$$A_\nu(e\gamma) = b_\nu A_\nu(\gamma\gamma) \quad , \qquad \text{(I-5)}$$

where $\nu = 2,4$. Using this definition, Equation (I-3) may be written in terms of b_ν:

$$W_{e\gamma}(\theta) = 1 + b_2A_2(\gamma\gamma)P_2(\cos\theta) + b_4A_4(\gamma\gamma)P_4(\cos\theta) \quad . \qquad \text{(I-6)}$$

The particle parameters will depend on the energy, E, and multipolarity, EL or ML, of the converted transition, the atomic number, A, and on the shell from which the electron is converted. The particle parameters b_2 and b_4 are not independent and Rose (13) has given the relationship between the two parameters. The experimental b_2 parameter is generally obtained from the defining equation using measured $A_2(e\gamma)$ and $A_2(\gamma\gamma)$

coefficients:

$$b_2 = A_2(e\gamma)/A_2(\gamma\gamma) \quad . \qquad (I\text{-}7)$$

Since the A_4 coefficients are generally small they cannot be measured with sufficient precision to yield b_4 parameters which can be compared to theoretically calculated parameters.

Gamma-gamma and electron-gamma directional correlations are sensitive to slight admixtures of higher multipole radiation in either transition of the cascade. Two types of gamma transitions involving significant multipole mixing have been observed experimentally, the M1 + E2 and E1 + M2 transitions. In a cascade involving pure and mixed transitions, if the pure transition is converted, the particle parameter obtained from Equation (I-5) is unaffected by the mixed transition. If the converted transition is mixed, the measured particle parameter does not lend itself to a simple theoretical interpretation. The theoretical expression for the measured parameter will depend on the sign and magnitude of the mixing amplitude and the internal conversion coefficients of the transition (2).

If the lifetime of the intermediate state of the nucleus is sufficiently long, the orientation of the nuclear spin axis may be perturbed and the measured correlation attenuated. The correlation will be altered if the magnetic dipole moment of the nucleus interacts with an extranuclear magnetic field or if the electric quadrupole moment interacts with electric field gradients (2). Whether the correlation is attenuated or not will depend on the magnitudes of the moments as

well as the presence of the fields in the nuclear environment.

For sources in solid form the fields are usually static crystalline fields which are strongly inhomogeneous. Dipole and quadrupole coupling to static fields alter the nuclear spin orientation by causing precession around the local field and field gradient axis respectively.

When the attenuating interactions are of this type, unattenuated particle parameter values may still be obtained from measurements of the attenuated directional correlation. In the expression for the attenuated correlation function, each expansion coefficient is a product of A_ν, the coefficient for the unattenuated correlation, and an attenuation factor G_ν (26):

$$W(\theta) = 1 + G_2A_2P_2(\cos\theta) + G_4A_4P_4(\cos\theta) \quad . \qquad \text{(I-9)}$$

If the same source is used for both gamma-gamma and electron-gamma correlations, the perturbing fields will be the same and the same attenuation factor will appear in Equations (I-3) and (I-4). The common attenuation factor which would multiply both sides of Equation (I-5) cancels leaving the measured particle parameter unaffected.

There are two attenuating mechanisms which may alter the particle parameter determined from Equation (I-7). They are attenuations which act exclusively on the electron-gamma correlation altering $A_2(e\gamma)$ while $A_2(\gamma\gamma)$ is unaffected. A conversion electron directional correlation will be attenuated if the direction of emission of the electron is altered by scattering in source material. Corrections have been worked out by Frankel (23) for scattering in cylindrically symmetric sources. Source

scattering can usually be reduced to a negligible level if sufficiently thin sources can be constructed. The second type of attenuation is a consequence of the vacancy produced in the electronic shell structure of the atom by the internal conversion process. The attenuation mechanism is a time dependent hyperfine structure interaction between the nuclear spin and the disrupted electronic shell structure (24). The time required for the shell structure of the ionized atom to recover must be sufficiently long to permit the interaction to cause disorientation of the nuclear spin. This recovery time will depend on the availability of free electrons to neutralize the ion. Therefore attenuation will most likely occur when source atoms are in an insulating environment and recovery times are long. Although an experimental study of directional correlations in Hg^{197} by Pettersson et al. (24) seems to have established the existence of an attenuation of this type, the effect has not been found in other correlation studies (25). The attenuation would obviously affect only directional correlations in which the first transition in the cascade is internally converted since conversion of the second transition would not affect the intermediate state.

Electron particle parameters are calculated theoretically from the same radial conversion matrix elements which appear in the internal conversion coefficients (26). However, the particle parameters involve ratios of the matrix elements rather than the squares of the matrix elements found in the conversion coefficients. The particle parameters are therefore a more sensitive measure of the conversion process.

Matrix elements for K-shell conversion and the resulting parameters have been calculated numerically using exact relativistic

wave functions for the bound and continuum states of the electron in the unscreened Coulomb field of a point nucleus by Rose and Biedenharn (13). These K shell particle parameters were calculated for all nuclear transition energies and multipolarities of interest and for the complete range of atomic numbers. The conversion matrix elements and resulting particle parameters based on the point-nucleus approximation are discussed briefly in Appendix A. Band et al. (27) have computed K and a few L shell particle parameters using numerically calculated radial matrix elements (28) which have been corrected for screening and finite nuclear size effects.

The finite size of the nucleus has two distinct effects on the particle parameter, one static and the other dynamic in nature. The static effect is simply the modification of the electron wave functions, which results when the point nucleus-model is abandoned. The dynamic effect arises from the penetration of the electron into the nuclear volume and must be interpreted in terms of a specific model for the structure of the nucleus. The anamolously large penetration effects observed experimentally for E2 transitions in certain heavy nuclei (17) and for E1 and M1 retarded transitions (16) are not accounted for by the surface-current model employed by Sliv and Band to correct for penetration effects (18).

The calculations of L-shell parameters have been extended by Listengarten et al. (29), Miranda et al. (30), and Hornshøj et al. (31). The radial matrix elements of Sliv and Band (28), (32), and therefore the resulting particle parameters for L conversion electrons, are available only for dipole and quadrupole transitions for a limited

range of atomic numbers and for transition energies up to 360 keV.

Calculations by Ustinova (33) have shown that static finite size corrections to K shell particle parameters for pure E1, E2, and M4 transitions are generally of the order of 1 per cent or less, except for low energy E2 transitions in high-Z materials where the corrections are about 5 per cent.

In a recent article by Hornshøj et al. (31), L-shell particle parameters computed in the point-nucleus approximations were compared with those corrected for screening and finite nuclear size. Comparing the L-shell parameters at Z = 77 for E1 and E2 multipole transitions, the finite size and screening corrections were found to be of the order of 1 per cent or less.

The results of experimental particle parameter measurements have been reviewed in detail in the article by Hornshøj et al. (31) and in an earlier article by Deutsch and Hornshøj (34). The experimental K shell particle parameters for E1, E2, and M4 transitions are in good agreement with the parameters calculated by Rose and Biedenharn (13), confirming the calculations of Ustinova. The experimental K-shell parameters were measured for pure multipole transitions in which no anomalous penetration effects were anticipated. Such experimental verifications seem necessary if anomalous penetration effects are to be distinguished from screening and static nuclear size effects.

The experimental data on L shell particle parameters are still rather limited. In the measurements which have been reported, resolution of L- and M-shell electrons varies widely. In some instances, the reported parameters are for unresolved L- and M-shell electron (32), (35),

and in other cases, the L subshells have been resolved (36), (37).

Purpose of the Research

The purpose of the present research is to determine conversion electron particle parameters from the measurement of directional correlations for cascades in Pb^{207} and Cs^{133}. By resolving electrons according to the shell from which they are converted, it is hoped that L shell particle parameters from the measurements can be compared with theoretically computed parameters available in the literature. The transitions to be studied are the 1064 keV (M4)-570 keV (E2) cascade in Pb^{207} and the 356 keV (E2)-81 keV (M1) cascade in Cs^{133}. These transitions are de-excitations in Pb^{207} and Cs^{133} which follow the decays of Bi^{207} and Ba^{133} by orbital electron capture. The decay schemes for Bi^{207} and Ba^{133} are shown in Figures 1 and 2 respectively. Particle parameters are to be determined for both E2 and M4 transitions in Pb^{207} and the E2 transition in Cs^{133}.

The 1064-keV and 570-keV Transitions in Pb^{207}

The decay of Bi^{207} by electron capture to Pb^{207} was discovered by Neumann and Perlman (38). The decay scheme has been established primarily by the work of Alburger and Sunyar (39). The 0.13 nanosecond half life of the 570-keV state, which is the intermediate state of the 1064 keV-570 keV cascade, has been recently measured by Körner *et al.* (40).

The gamma-gamma directional correlation of the cascade has been measured by McGowan and Campbell (41), Gustafsson *et al.* (42), Körner *et al.* (4), and Kleinheinz *et al.* (43). The results of these measurements

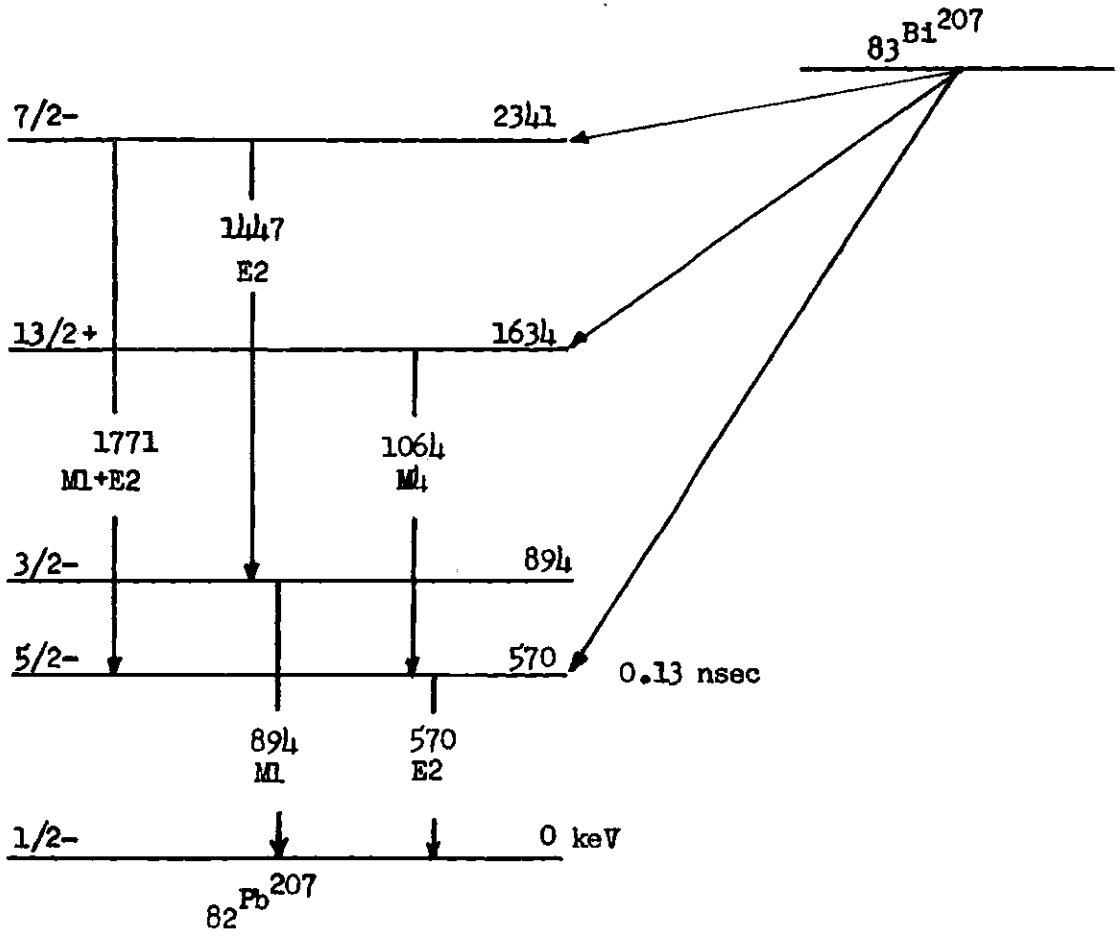

Figure 1. Decay Scheme of Bi^{207}

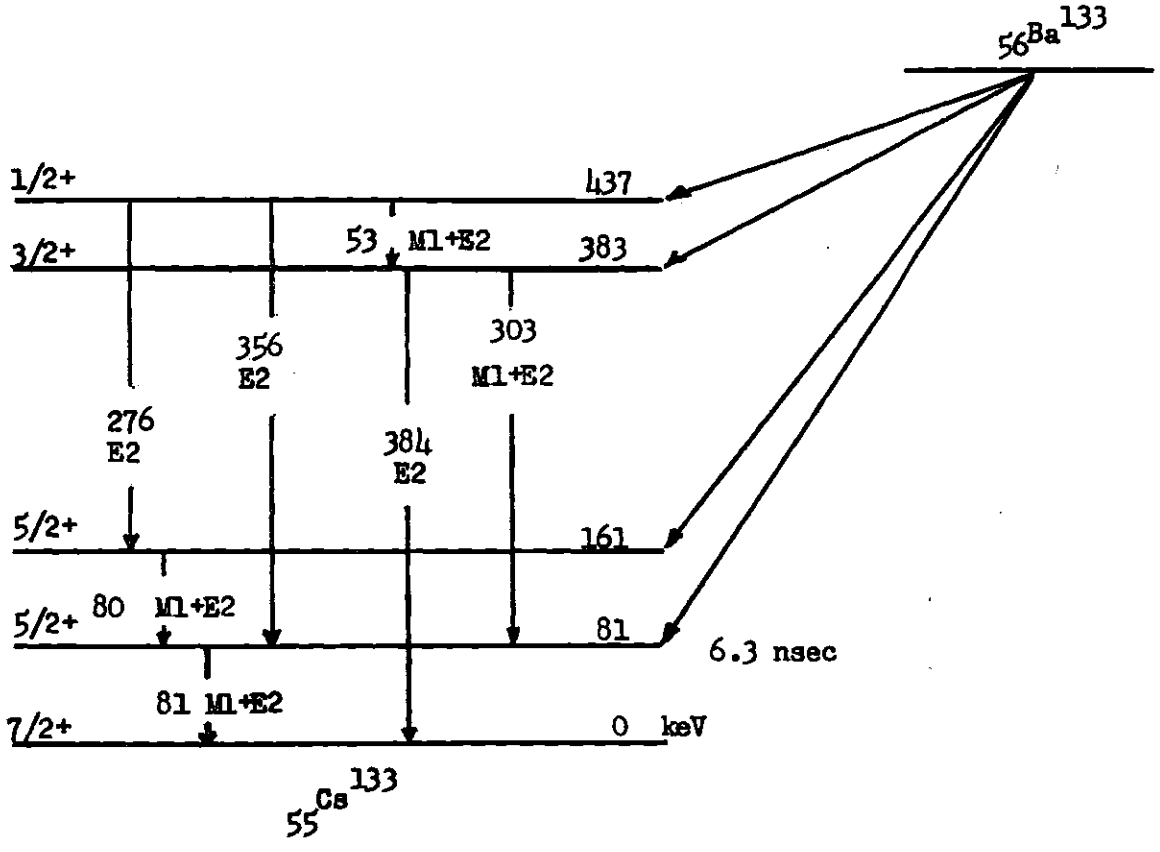

Figure 2. Decay Scheme of Ba^{133}

show that the 1064-keV transition is a pure M4 transition with an E5 content of less than 0.1 per cent, and the 570-keV transition is a pure E2 transition with an M3 content of less than 0.1 per cent.

The electron-gamma correlation involving K electrons has been measured by McGowan (44), and more recently by Kleinheinz et al. (45) who also measured the correlation for unresolved L- and M-shell electrons. The K shell particle parameters for the 1064 keV (E2) transition obtained from these measurements are in agreement with the recent theoretical calculations by Hornshøj et al. (32). Separate particle parameters for K-shell and unresolved L- and M-shell electrons of the 570-keV transition are reported by Kleinheinz et al. from a measurement of the gamma-electron correlation.

The 356-keV and 81-keV Transitions in Cs^{133}

The decay scheme for Ba^{133} shown in Figure 2 is based on the results of a number of studies (45), (46), (47), (48), (49), (50). The 6.31 ± 0.05 nanosecond half life of the 81-keV transition has been determined by Bodenstedt et al. (45) by measurement of delayed coincidences between gamma rays of the 356- and 81-keV transitions. The E2 character of 356-keV transition has been verified recently by conversion intensity measurements (50), (51). An upper limit of 1 per cent has been placed on the M3 content of 356-keV transition by L-subshell intensity measurement by Hennecke et al. (50).

The 81-keV transition is a mixed M1 + E2 transition in which the E2 content is 2.7 ± 0.2 per cent based on L-shell conversion intensities (52), (53).

The 356 keV-81 keV, gamma-gamma directional correlation has been measured by a number of investigators (45), (46), (48), (49), (54), (55), (56), (57), (58). No attenuation of the correlation by extranuclear fields has been detected (45). The electron-gamma directional correlation involving K-shell electrons of 356-keV transition have been reported recently by Meder et al. (57), Avignone et al. (48), and Thun et al. (49). The K shell particle parameters obtained from these measurements are in agreement with the theoretical value for a pure E2 transition and are compared with the present measurements in Chapter IV.

CHAPTER II

EXPERIMENTAL APPARATUS

The experimental apparatus used in directional correlation measurements is referred to as a directional correlation spectrometer. The spectrometer used in this experiment detected and recorded coincidences between gamma rays and conversion electrons of selected energies. The spectrometer consisted of scintillation and solid state detectors, amplifiers, pulse height analyzers, coincidence circuits, and data recording equipment.

In the electronic circuitry, the fast-slow coincidence technique was employed in the analysis of signals from the detectors. In this technique a fast-coincidence circuit (i.e., one with a short resolving time) registers coincidences between electron and gamma detector signals irrespective of their pulse heights. Two subsequent slow-coincidence circuits restrict these coincidences to events between electron and gamma signals of selected pulse heights. These pulse height restrictions are equivalent to a selection of the radiations by their characteristic energies.

The efficiency of the experiment was increased by making two simultaneous correlation measurements on the same source. Signals from two gamma detectors were analyzed simultaneously with signals from a single electron detector. The use of two gamma detectors positioned at different angles made the correlation measurements less sensitive to instrumental drifts (59).

Radiation Detectors

Two scintillation counters, manufactured by Nuclear Diodes, Incorporated, were employed for gamma-ray measurements. These detectors consisted of 3X3-inch NaI(Tl) crystals optically coupled to RCA Type 8054 photomultiplier tubes. They were provided with mu-metal magnetic shields and were preassembled by the manufacturer. The photomultiplier tubes were operated at about 1200 volts.

A Technical Measurement Corporation Type W-80-2A lithium drift silicon detector was used for electron detection. This detector was essentially a large area junction diode consisting of a thin, less than 0.5 micron, p-type layer on a thick region of highly compensated silicon. The radiation sensitive junction or depletion region was two millimeters deep. The detector was operated as a reverse-biased diode at 200 volts. The area of the exposed face of the detector was 1.3 cm^2. This area was larger than the sensitive surface area quoted by the manufacturer. Therefore a lucite mask was placed over the face of the detector to define precisely the area presented to the radioactive source. The mask exposed a circular, 0.8 cm^2, area of the detector face to the incident conversion electrons. When operated at room temperature, the energy resolution of the electron detector was degraded by thermal noise. To reduce this noise the detector was cooled by placing it in thermal contact with a reservoir of dry ice and acetone.

Counting Geometry

The experimental counting geometry is illustrated in Figure 3. Two gamma detectors were mounted on separate frames which could be

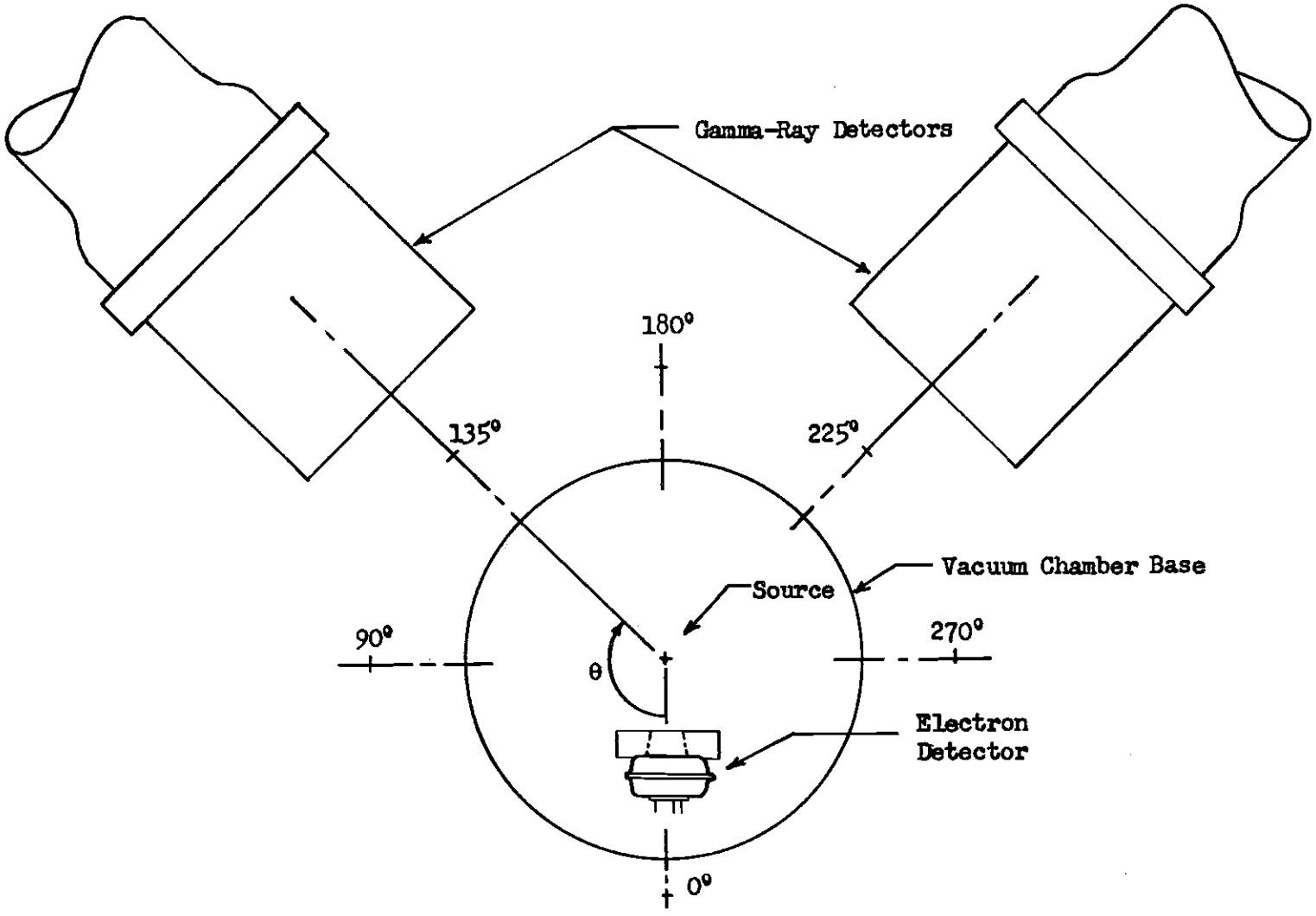

Figure 3. Experimental Counting Geometry

rotated about an axis through the source. The angle θ, in Figure 3, is the angle between the symmetry axis of the electron detector and that of one of the gamma detectors. For both gamma detectors this angle was variable from 90 to 270 degrees by either manual rotation or by interchanging the positions of the two detectors.

Vacuum Chamber Housing

In order to prevent scattering of the conversion electrons by air molecules, both the source and electron detector were enclosed in a cylindrical vacuum chamber. Only the circular cross section of the chamber base is indicated in Figure 3. Figure 4 is a photograph of the experimental apparatus. Gamma rays from the source passed through the chamber wall to reach the detectors outside the chamber. The wall thickness was about one millimeter and was designed to minimize scattering and absorption without weakening the mechanical structure of the chamber.

The interior of the chamber is exposed in the cutaway view in Figure 5 showing the location of the electron detector and the source. The bias voltage was supplied to the detector and signals obtained from it through a vacuum sealed electrical connector located in the base of the chamber. The dry ice and acetone reservoir, required for cooling the electron detector, was mounted on top of the vacuum chamber as shown in Figures 4 and 5.

Electronics

A block diagram of the electronic instrumentation employed in the correlation spectrometer is shown in Figure 6. In this arrangement

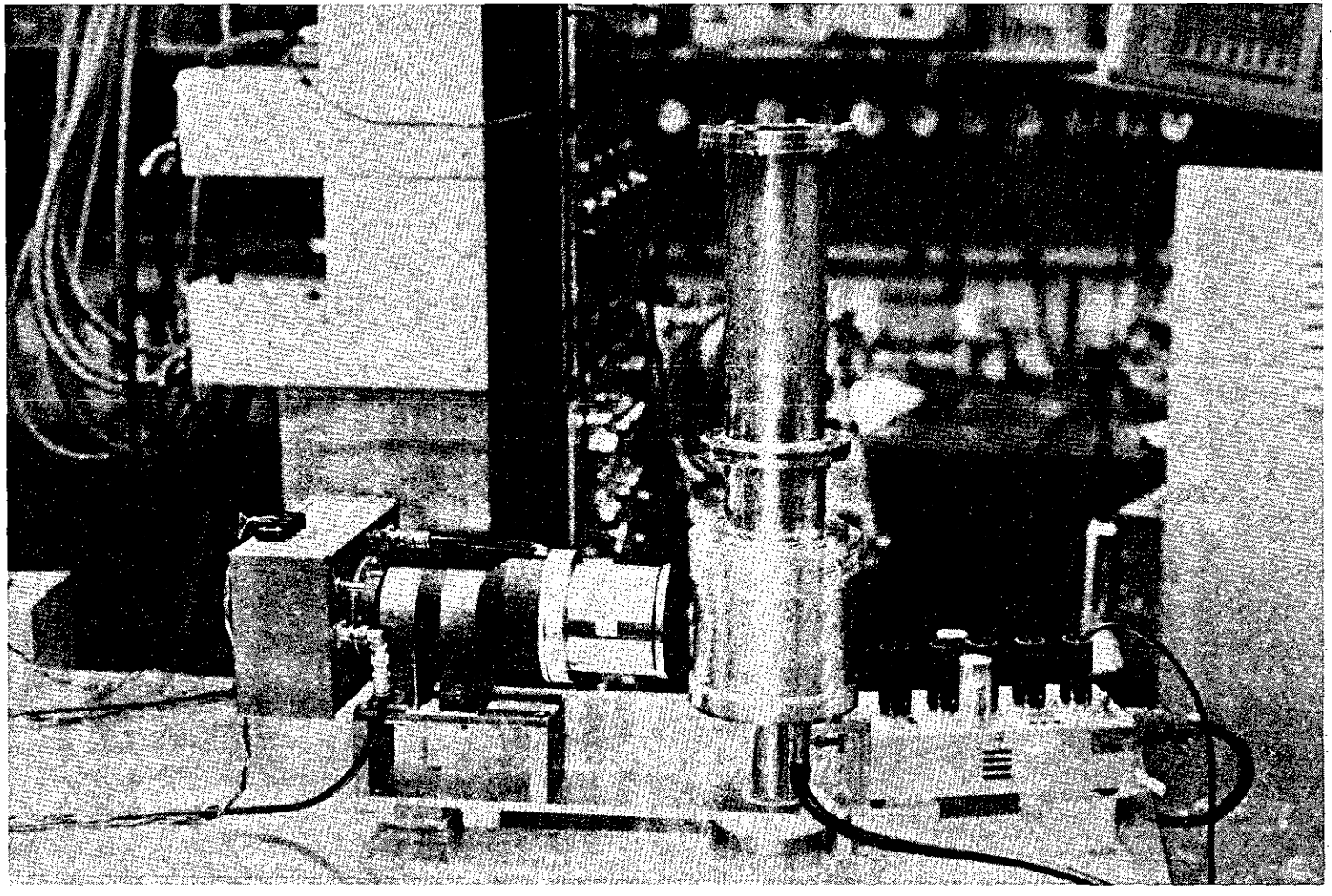

Figure 4. Photograph of Experimental Apparatus

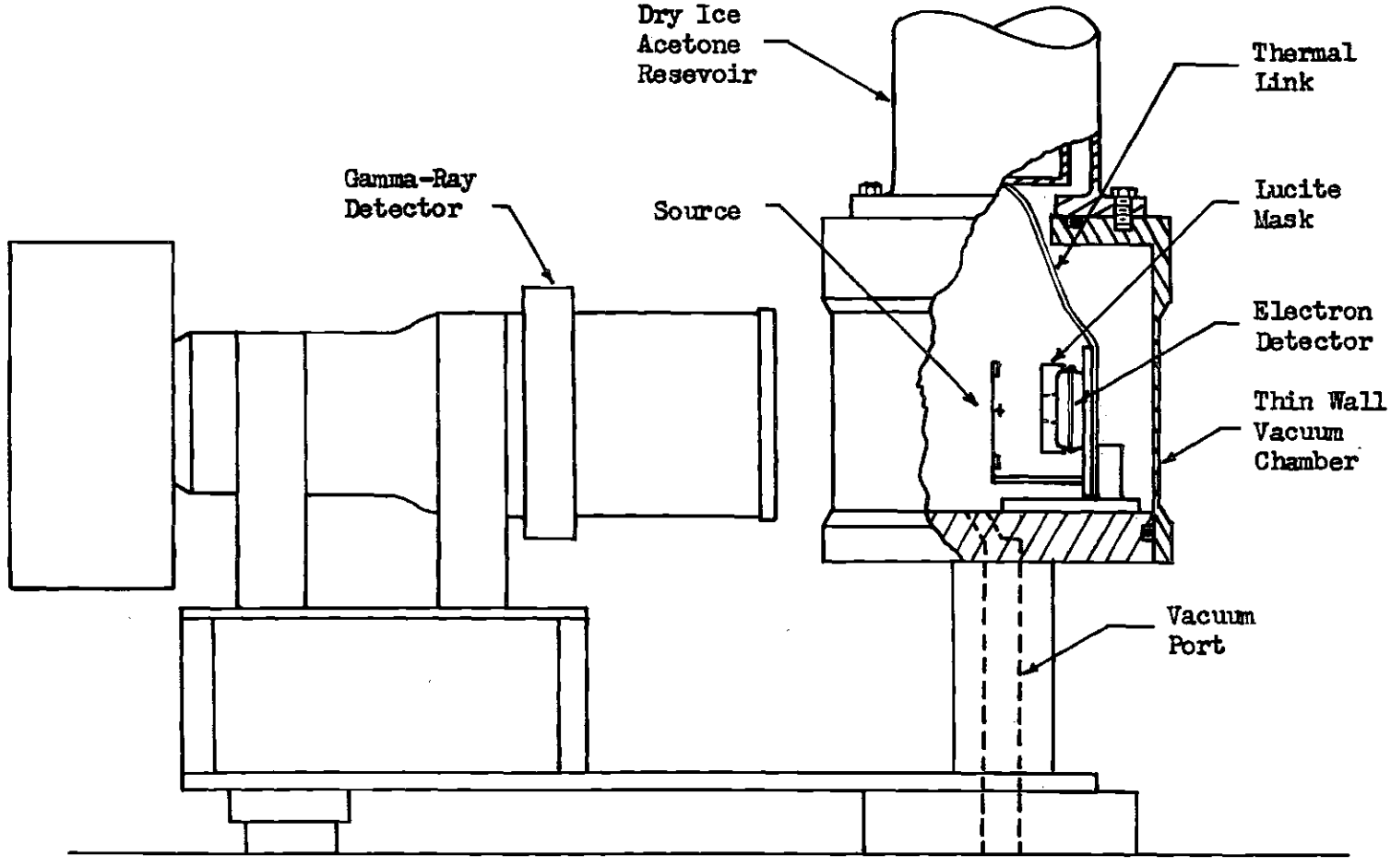

Figure 5. Cutaway View of Vacuum Chamber

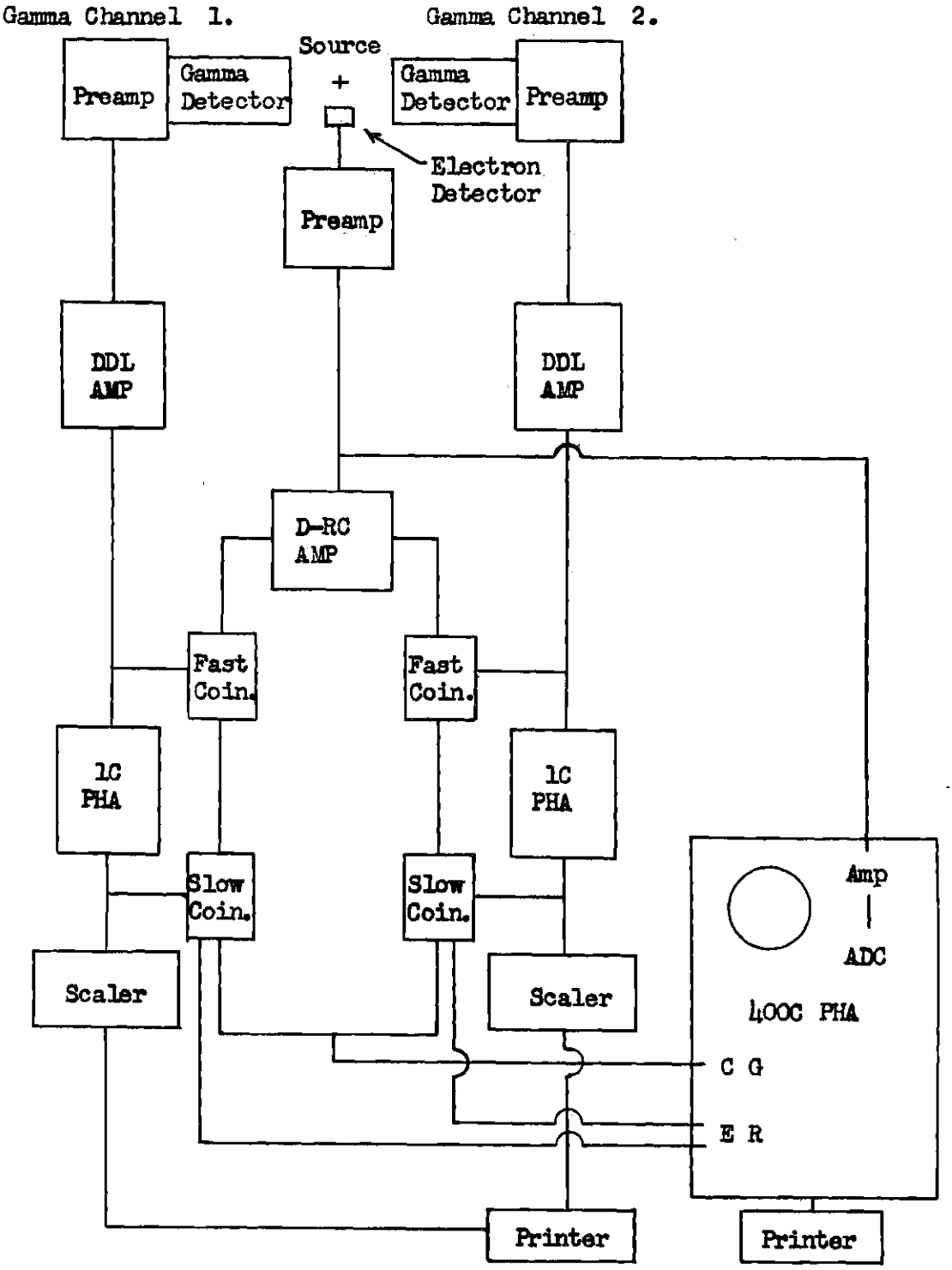

Figure 6. Block Diagram of the Electronic Instrumentation

a 400 channel pulse height analyzer with coincidence gating was utilized as an integral part of the fast-slow coincidence circuitry (60). The 400 channel pulse height analyzer was a Packard Instrument Company Model 116. Inputs were available for the external routing of coincidence signals to selected channel groups in the memory (e.g., two groups of 200 channels). This feature permitted the analyzer to be utilized with both gamma detectors in carrying out simultaneous correlation measurements.

The fast-coincidence timing analysis and slow-coincidence gamma-ray energy selection for both gamma channels were performed in solid state circuits external to the analyzer as illustrated in Figure 6. This part of the instrumentation was designed by Dr. E. T. Patronis, Jr., and the entire system was maintained by him. Double-delay-line and double-RC clipped main amplifiers provided bi-polar pulses for energy analysis and coincidence timing. The fast circuits contained variable electronic delays to compensate for differences in signal transit times in the electron and gamma detection circuits. The time resolution of the circuits was variable. Both coincidence channels were operated with resolving times of about 2τ = 80 nanoseconds. The gamma ray energy analysis was carried out in single channel pulse height analyzers. Double-coincidence signals, containing the fast timing and gamma energy information, were fed to the coincidence gating and external routing inputs of the 400 channel analyzer.

Electron detector signals from a Tennelec 100C charge sensitive preamplifier were fed to the analyzer for amplification and pulse

height analysis. The pulse-height analysis in the analyzer's analogue-to-digital converter sorted the electron signals into 200 energy channels. These digitized signals were gated into the analyzer memory to form a triple-coincidence spectrum when they were coincident with a double-coincidence signal applied at the coincidence gate. The triple coincidences were routed into separate halves of the memory depending on the gamma channel in which they occurred. Each half of the memory contained a 200 channel coincidence spectrum since the coincidences were between gamma signals in a single energy channel and electron signals in any one of 200 energy channels.

The coincidence spectra were printed directly from the memory on paper tape with a Franklin Electronics, Incorporated Model 1200 printer. Gamma signals from the single channel analyzers were recorded in Radiation Instrument Development Laboratory Model 49-44 scalers and printed on paper tape using a Hewlett Packard Model H44562A printer.

CHAPTER III

DIRECTIONAL CORRELATION MEASUREMENTS

Particle parameters for K-, L-, and M-shell electrons were deduced from electron-gamma, gamma-electron, and gamma-gamma directional correlation measurements. Each directional correlation measurement was an experimental determination of the A_2 and A_4 coefficients of the directional correlation function in Equation (I-2).

To determine the expansion coefficients, coincidences were recorded with the radiation detectors in three different counting positions as defined in Figure 3. Since the coincidence counting rate at each angular position was proportional to $w(\theta)$, the measurements constituted an evaluation of Equation (I-1) at three independent angular positions. The three coefficients a_o, a_2, and a_4 were obtained by a least squares fit of the data (61), (62). The A_2 and A_4 coefficients were then obtained directly from these coefficients.

The b_2 particle parameters deduced from the A_2 coefficients are discussed in Chapter IV. The experimental error in the A_4 coefficients did not permit a significant determination of b_4. However, the A_4 coefficients can be tentatively compared with theoretical values as a check of the consistency of the data and are therefore included in the tables in this chapter.

Each electron-gamma or gamma-electron directional correlation measurement required from two to five weeks. The same general procedure was followed in the conversion electron directional correlation

measurements for Pb^{207} and Cs^{133}. The conversion electron energy spectra and the general measurement procedure will be discussed before each specific directional correlation is considered.

Conversion Electron Energy Spectra

In order to obtain separate A_2 and A_4 coefficients corresponding to electrons converted from different atomic shells, the electrons were experimentally identified by their characteristic kinetic energies. The ability to distinguish between the electrons from different shells depended on the resolution of the electron detection system and fundamentally on the difference in binding energies between the atomic shells. The conversion electron energy spectra, for which the corresponding coincidence spectra were subsequently obtained, are discussed below.

The Converted 1064-keV and 570-keV Transitions in Pb^{207}

Figures 7 and 8 are the energy spectra of conversion electrons of the 570-keV and 1064-keV transitions in Pb^{207} obtained with the cooled lithium drift detector. The lines designated as "M" in each spectrum include contributions due to electrons converted from outer shells. The kinetic energies of the electrons may be obtained by subtracting the binding energy for each shell from the transition energy. The energy separation of the K- and L-conversion lines in both spectra is 72 keV. The separation between the L and M lines is 12 keV (63). In both spectra the energy resolution (full width at half maximum) of the K- and L-conversion lines is about 9 keV.

In Figure 7 the 570-keV conversion lines are superimposed on a constant electron background. This background is due primarily to recoil electrons which have been Compton scattered by gamma rays of the

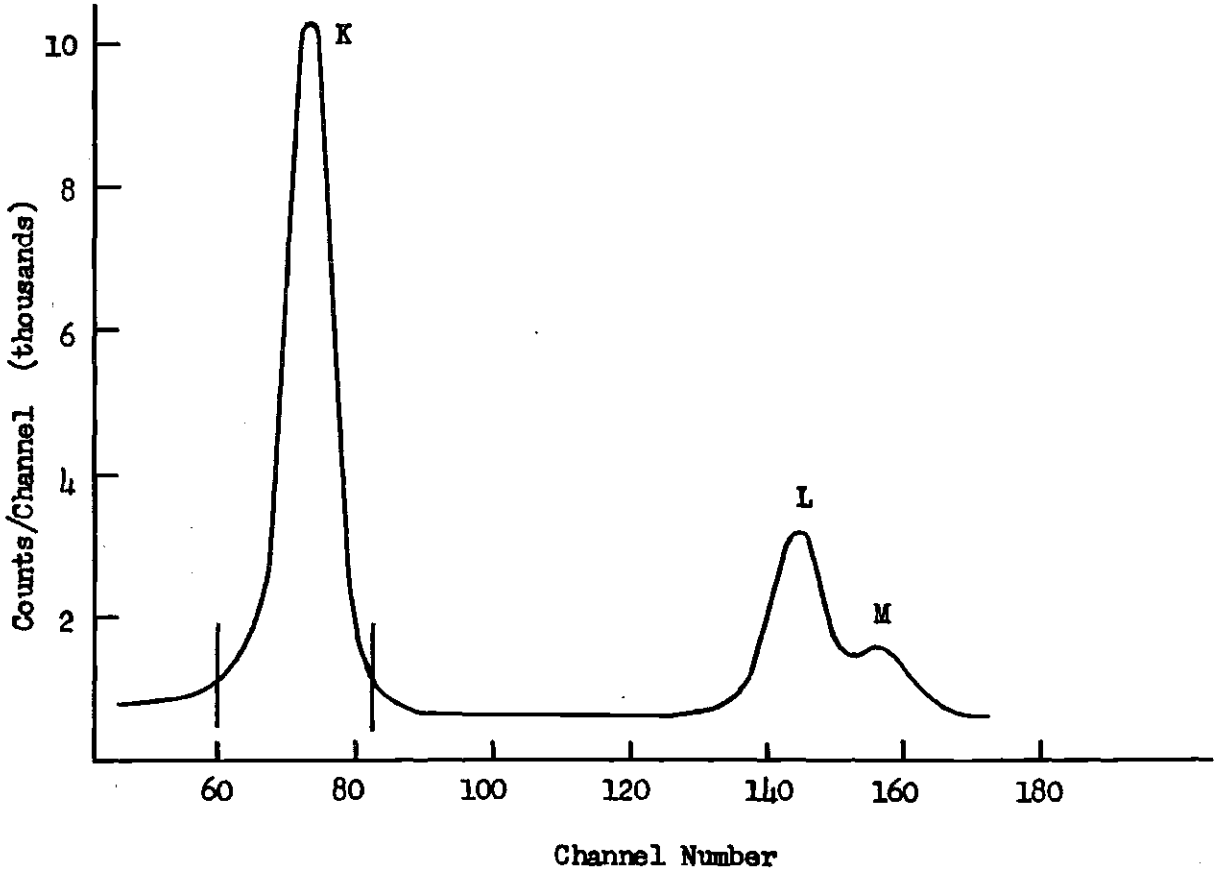

Figure 7. Conversion Electrons of the 570-keV Transition in Pb^{207}

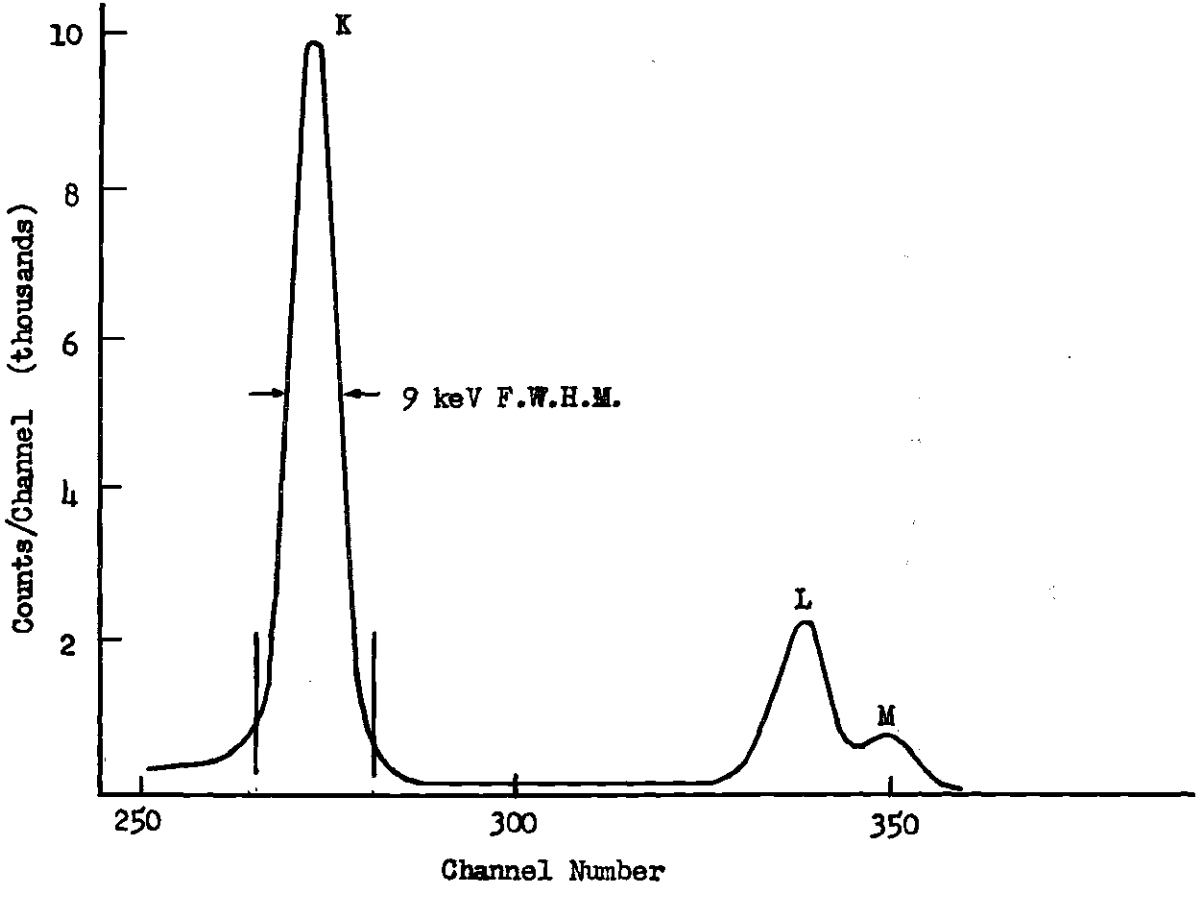

Figure 8. Conversion Electrons of the 1064-keV Transition in Pb^{207}

1064-keV transition, and to conversion electrons of the same transition which have backscattered from the detector.

The Converted 356-keV Transition in Cs^{133}

Figure 9 is the energy spectrum of the conversion electrons of Cs^{133} with kinetic energies near 320 keV. On the graph in Figure 9 the conversion lines are labeled by shell and transition energy. The kinetic energies of the L electrons converted in the 356-keV transition and the K electrons of the 380-keV transition are comparable and the two electron lines are unresolved. This line also includes the unresolved M-shell electrons of the 356-keV transition since the binding energy separation of the L and M shell is only about 4 keV (63). The 11-keV width of the K-conversion line is indicated in the figure.

The Conversion Electron Energy Resolution

The dominant contributions to the line width in each spectrum were from noise generated in the detector and the first stage of the preamplifier. These contributions to the line width were reduced by cooling the detector to reduce noise thermally generated in the detector's depletion volume, and by employing a low-noise Tennelec 100C preamplifier with the detector.

For the charge-sensitive preamplifier the signal-to-noise ratio was a decreasing function of the input capacitance (64). Therefore the resolution was also affected by the input capacitance of the preamplifier. The input capacitance included that of the detector and the stray capacitance of the electrical leads to the preamplifier. The length of the electrical leads were kept to a minimum consistent with the vacuum chamber design, in order to reduce their contribution to the input

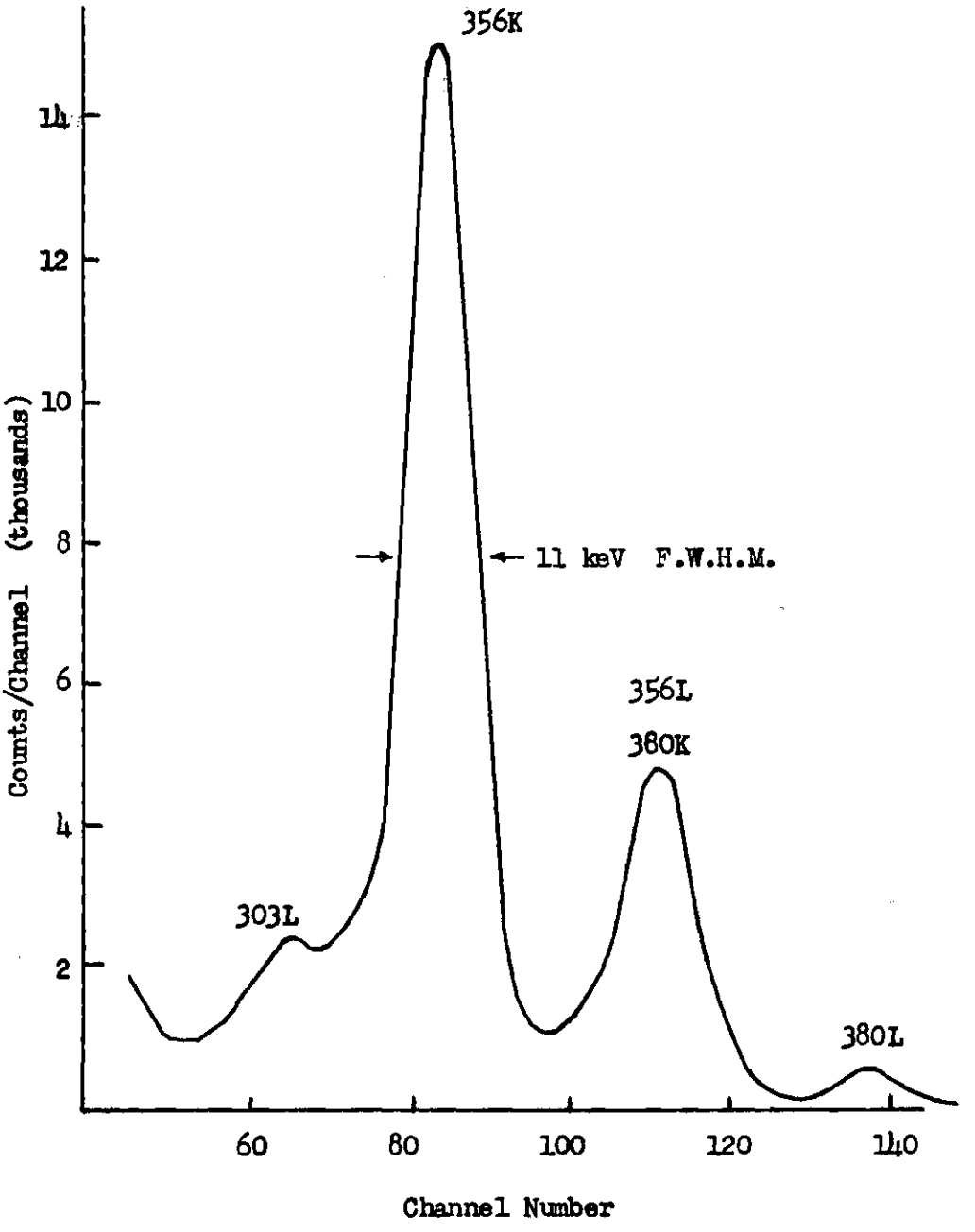

Figure 9. Conversion Electron Spectrum of Cs^{133}

capacitance.

Contributions to the line width from effects other than noise were negligible. Scattering of conversion electrons in the source material may contribute to the spread in their energies even before they reach the detection system. However, it is generally possible to reduce the scattering to a negligible level by careful source preparation starting with a high specific activity liquid sample. Scattering was assumed to be negligible in both the Pb^{207} and Cs^{133} sources used in the present measurement. The fundamental width of the lines in the energy spectra resulting from the natural width of the atomic states from which the electrons were converted was less than 0.1 keV for both Pb^{207} and Cs^{133} (65).

Drifts in gain caused by fluctuations in room temperature broadened the line width by less than 10 per cent even for extended counting periods as a result of the high stability of the preamplifier and the pulse height analyzer.

Measurement Procedure

All sources were prepared by depositing radioactive material on a thin sheet of mylar backing which was attached to a circular aluminum ring to provide mechanical rigidity. With the upper portion of the vacuum chamber removed, the source ring was mounted on an adjustable support at the center of the chamber. The source location is illustrated in Figure 5 in Chapter II.

Using a narrow window setting on the single-channel analyzer, the center of the gamma-ray line involved in the correlation was located in the analyzer window. The window was then widened to accept the entire

gamma line. The source was geometrically centered by adjusting its position until the gamma singles rates were equalized at the 90, 180, and 270 degree counting positions to within 2 per cent. Both gamma detectors were approximately eight centimeters from the source.

The distance from the source to the face of the electron detector was approximately 20 millimeters. This distance was measured before and after each correlation measurement to determine the solid angle correction for the electron detector. The measurement was made with a traveling microscope which had been visually aligned with the source-detector axis. This technique avoided damage to either the sensitive surface of the detector or the source.

The lucite mask was placed over the face of the electron detector and centered with respect to the source-detector axis. A flexible metal conductor was attached between the detector and cooling reservoir to provide a thermal link for cooling the detector. This link is illustrated in Figure 5. The vacuum chamber was evacuated to a pressure of 15 microns of Hg. The electron detector and gamma signals were time aligned by adjusting the variable electronic delays in the fast circuits until a maximum coincidence counting rate was obtained. This alignment was checked periodically during the measurements.

Coincidence spectra were accumulated in the 400 channel analyzer for counting periods averaging between two and four hours at five angular positions: 90, 135, 180, 225, and 270 degrees. Since the Legendre polynomials in Equation (III-1) are even, the 90- and 270-degree and the 135- and 225-degree positions are equivalent to one another. Comparisons of coincidences recorded at equivalent positions provided

a check of the symmetry of the counting geometry.

Due to the finite resolving time of the coincidence circuits the recorded spectra contained accidental as well as real coincidence events. The number of accidental events was determined by time delaying the electron detector signals in the fast coincidence circuits by 0.4 microsecond so that no real coincidences could be recorded. Accidental-coincidence spectra were recorded periodically throughout each correlation measurement.

In each coincidence spectrum, a line generated by coincidences involving electrons from a particular shell was evaluated by summing the coincidence channels of which it was composed. To compensate for small gain drifts in the gamma detector channels, the coincidences were normalized by dividing them by the gamma singles rate. They were also normalized to a common counting interval. An average coincidence rate for each conversion line was obtained for each counting position by weighting individual measurements according to the number of coincidences recorded.

An outline of the analysis required to extract the A_2 and A_4 coefficients from the normalized coincidence rates and a sample calculation are presented in Appendix B. The correction of the A_2 and A_4 coefficients for attenuation due to the finite solid angles of the detectors is outlined in Appendix C.

Directional Correlations in Pb^{207}

For directional correlation measurements in Pb^{207}, a 20 microcurie Bi^{207} source was purchased from New England Nuclear Corporation. The source material was deposited on 1/4 mil aluminized mylar, and

distributed over an area six millimeters in diameter.

On the basis of the translucent appearance of the source and the high resolution of the electron energy spectra, shown in Figures 7 and 8, the source was assumed to be sufficiently thin that electron scattering in the source did not alter the directional correlation.

Figure 10 is the gamma ray energy spectrum recorded with the 400-channel analyzer with one of the scintillation detectors at eight centimeters from the source. A spectrum with approximately the same resolution was obtained with the second gamma detector in the same counting geometry. The magnetic shielding of the detectors was sufficient to cancel fields in the neighborhood of the counters since no measurable shifts in the gamma lines were noted when the detectors were rotated.

The 1064 keV Electron-570 keV Gamma Directional Correlation

The gamma rays selected in the window of the single channel analyzer are indicated in the gamma energy spectrum in Figure 10 by the vertical lines on either side of the 570-keV line. Spectra composed of these gamma rays coincident with the conversion electrons of the 1064-keV transition were recorded simultaneously for both gamma detectors.

Coincidences were accumulated in each half of the memory of the 400-channel analyzer for two hour intervals before being printed out. Thirty coincidence spectra were recorded for each of the three independent counting geometries. The $A_2(e_K\gamma)$ and $A_4(e_K\gamma)$ coefficients were evaluated from coincidences recorded in a group of channels spanning almost the entire K-conversion line. The selected channel group extended far enough on either side of the center of the line to

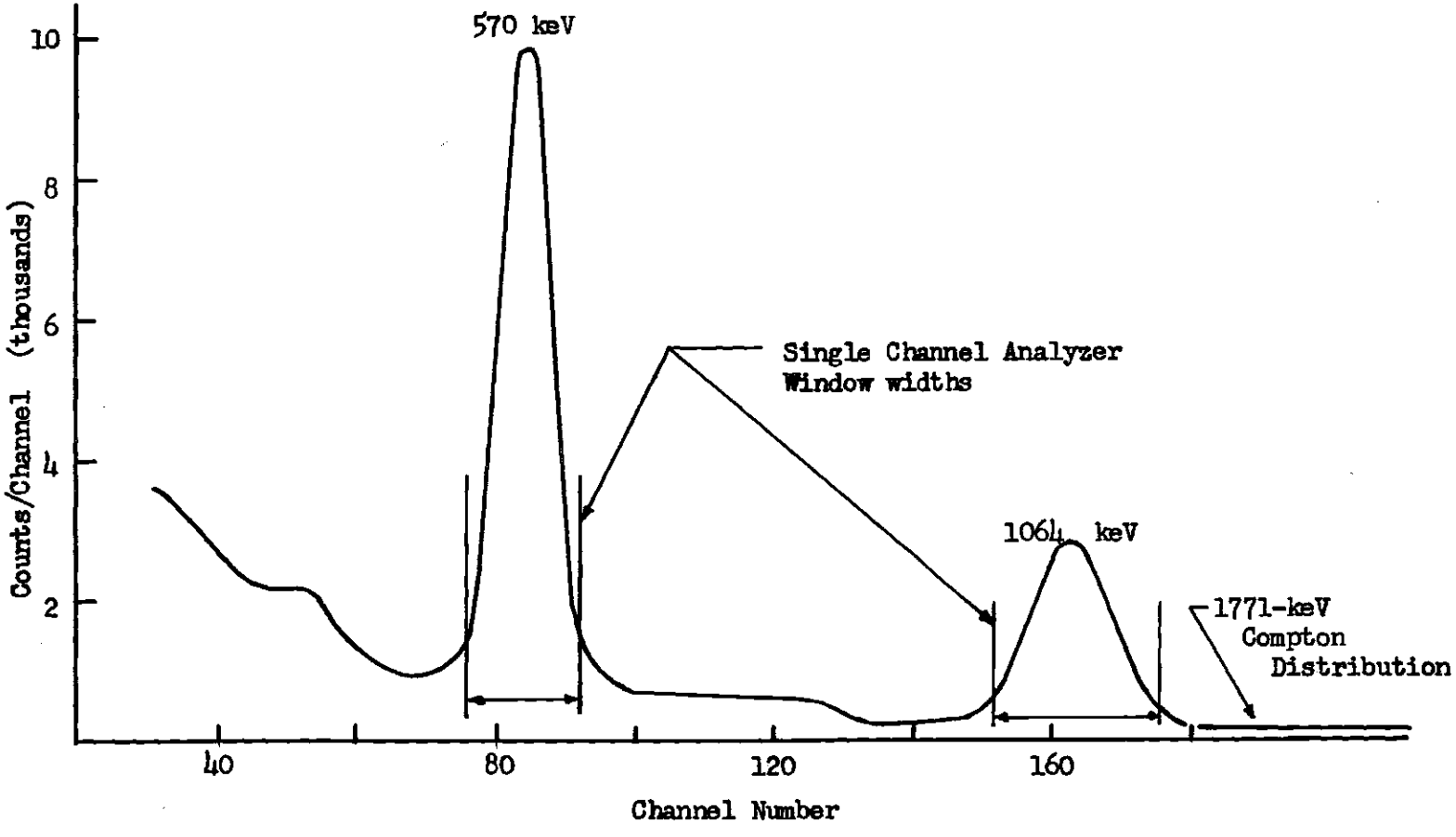

Figure 10. Pb^{207} Gamma Ray Spectrum

limit the effect of minor drifts in the electron detection channel. The two extremes of this group are indicated in Figure 7 by the vertical lines on either side of the K-conversion line.

The A_2 and A_4 coefficients for L- and M-shell electrons were obtained in a similar manner. The groups selected for the separate analyses for the L-shell and M-shell electrons are shown in Figure 11. This figure is simply an enlarged graph of the L- and M-conversion lines of Figure 7. The line designated as "M" includes electrons converted from outer lying atomic shells.

The dashed curves in the figure indicate the degree of separation between the L- and M-shell electrons. An approximate M-line shape was obtained by fitting a K conversion line shape to the M peak in the recorded spectrum. The L-line shape was then obtained by graphical subtraction of the M line from the composite spectrum.

A period of about two weeks was required to accumulate 10^5 total coincidences (real plus accidental) in the channel groups spanning the K line for each of the three counting geometries. The total coincidences recorded for the L- and M-conversion electrons were approximately $25X10^3$ and $6.5X10^3$ counts respectively. The real to accidental ratios for each of the three channel groups was about 19 to 1.

The A_2 and A_4 coefficients for the K, L, and M directional correlation functions are listed in Table 1. The two values for each coefficient were extracted separately from data recorded simultaneously with the spectrometer's two gamma detection channels. The coefficients listed in column one are uncorrected for geometric attenuation and the errors listed are probable statistical errors based on a statistical

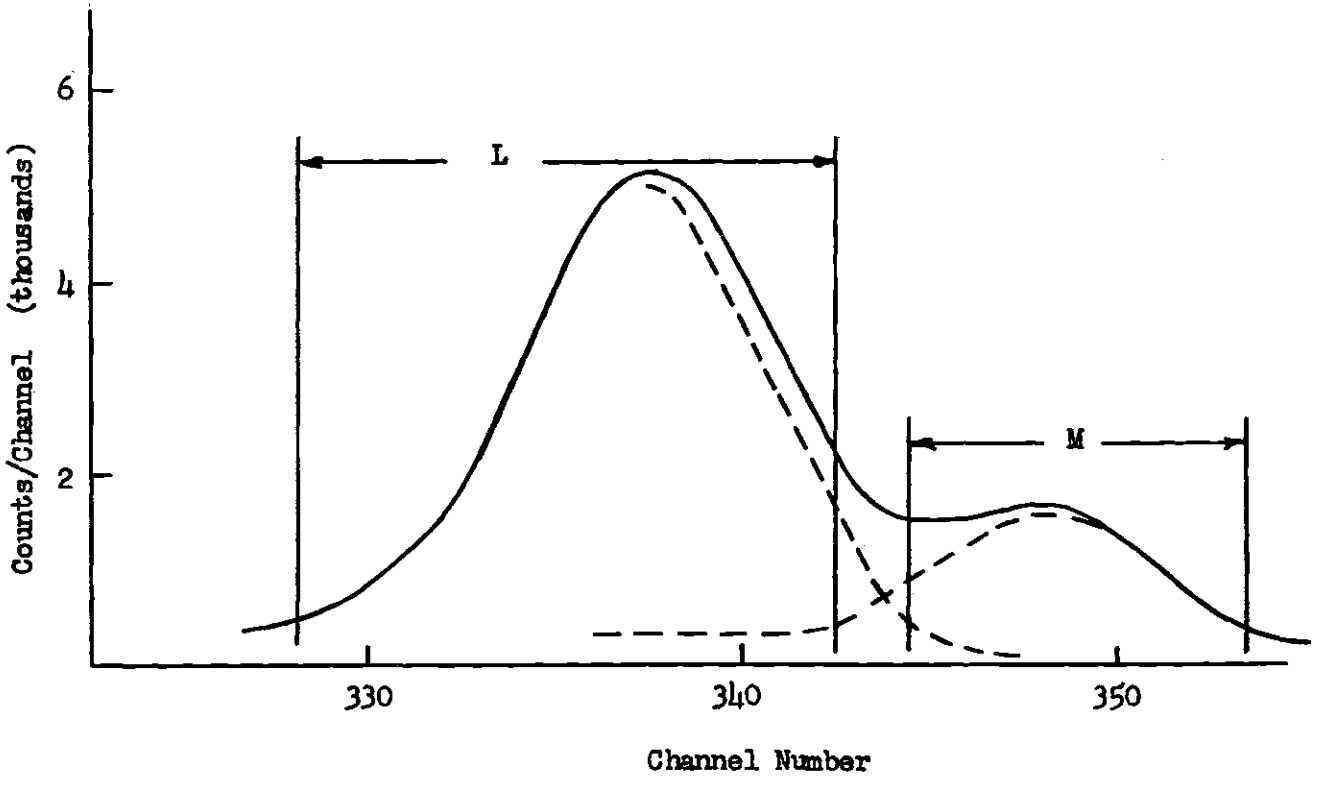

Figure 11. L and M Shell Conversion Electrons of the 1064-keV Transition in Pb^{207}

Table 1. The A_2 and A_4 Coefficients for the e(1064)-γ(570) Directional Correlations in Pb^{207}

Directional Correlation	Gamma Detection Channel	Uncorrected	Solid Angle Corrected	Combined Data
e_K(1064)-γ(570)	1	A_2 0.205(5) A_4 - 0.025(7)	0.233(9) - 0.039(11)	A_2 0.23(6) A_4 - 0.032(8)
	2	A_2 0.203(5) A_4 - 0.015(8)	0.230(9) - 0.023(13)	
e_L(1064)-γ(570)	1	A_2 0.217(11) A_4 0.006(18)	0.246(14) 0.01(3)	$^*A_2$ 0.246(14) $^*A_4$ 0.01(3)
	2	A_2 0.187(13) A_4 - 0.01(2)	0.212(16) - 0.01(3)	
e_M(1064)-γ(570)	1	A_2 0.20(3) A_4 - 0.02(4)	0.23(3) - 0.02(6)	A_2 0.23(2) A_4 - 0.00(4)
	2	A_2 0.20(3) A_4 0.011(4)	0.23(3) - 0.02(6)	

*Data from Gamma channel number one only (see text).

analysis of the recorded data. The coefficients in column two have been corrected for geometric attenuation as discussed in Appendix C. The error listed in column two includes the estimated error in the geometric attenuation factors. In column three the values obtained in the two gamma detection channels have been combined. With the exception of the expansion coefficient for the L-shell electrons, the results listed in column three were obtained by weighting the two separate values inversely as the square of their errors.

For the L-shell coefficient, $A_2(L)$, the value listed in column three is the value obtained from the data recorded in gamma channel number one, rather than the combined result for both gamma detectors. The smaller $A_2(L)$ value, obtained from the data recorded in gamma channel two, was rejected on the basis of results obtained from preliminary correlation measurements using a thick Bi^{207} source. These measurements have shown that $A_2(K)/A_2(L+M)$ is 0.88 ± 0.07, whereas using the smaller $A_2(L)$ value and $A_2(K)$ obtained in the present measurement would yield a value of 1.09 ± 0.09 for the ratio $A_2(K)/A_2(L)$. The $A_2(L)$ value obtained in gamma channel one yields 0.94 ± 0.06 for this ratio which is in better agreement with the $A_2(K)/A_2(L+M)$ ratio.

The 1064 keV Gamma-570 keV Electron Directional Correlation

The gamma rays selected in the single channel analyzer for the coincidence analysis are indicated in the gamma energy spectrum by the vertical lines on either side of the 1064-keV gamma peak. The recorded coincidence spectra were composed of these gamma rays coincident with the conversion electrons of the 570-keV transition. Approximately 5 per cent of the gamma rays accepted in the window of the single

channel analyzer arose from the Compton distribution of the 1771-keV transition underlying the 1064-keV photopeak.

These gamma rays contributed a coincidence background to the measurement of the 1064 keV gamma-570 keV electron directional correlation. The correction of the A_2 coefficient for this coincidence background amounted to approximately 5 per cent. The correction is discussed in detail in Appendix D.

The constant electron background observed in Figure 8 did not contribute to the coincidence spectra since these electrons were not coincident with gamma rays selected in the single channel analyzer.

Coincidences were accumulated in the memory of the 400-channel analyzer for counting intervals ranging from three to twelve hours. The K-shell electrons selected for the evaluation of the $A_2(\gamma e_K)$ and $A_4(\gamma e_K)$ coefficients are indicated in Figure 8 by vertical lines on either side of the K peak.

The electron channel groups selected for determining the A_2 and A_4 coefficients for the L- and M-shell directional correlations are shown in Figure 12. The total coincidences recorded for K-, L-, and M-shell electrons were $12X10^4$, $3X10^4$, and $7X10^3$ counts respectively. The real to accidental ratios for the K-, L-, and M-shell channel groups were 14 to 1, 12 to 1, and 7 to 1 respectively.

The A_2 and A_4 coefficients for the K, L, and M directional correlations are listed in Table 2. The coefficients listed in column 3 were obtained by weighting the two values obtained in separate gamma channels inversely as the square of their errors. In column 4 the coefficients have been corrected for the coincidence background

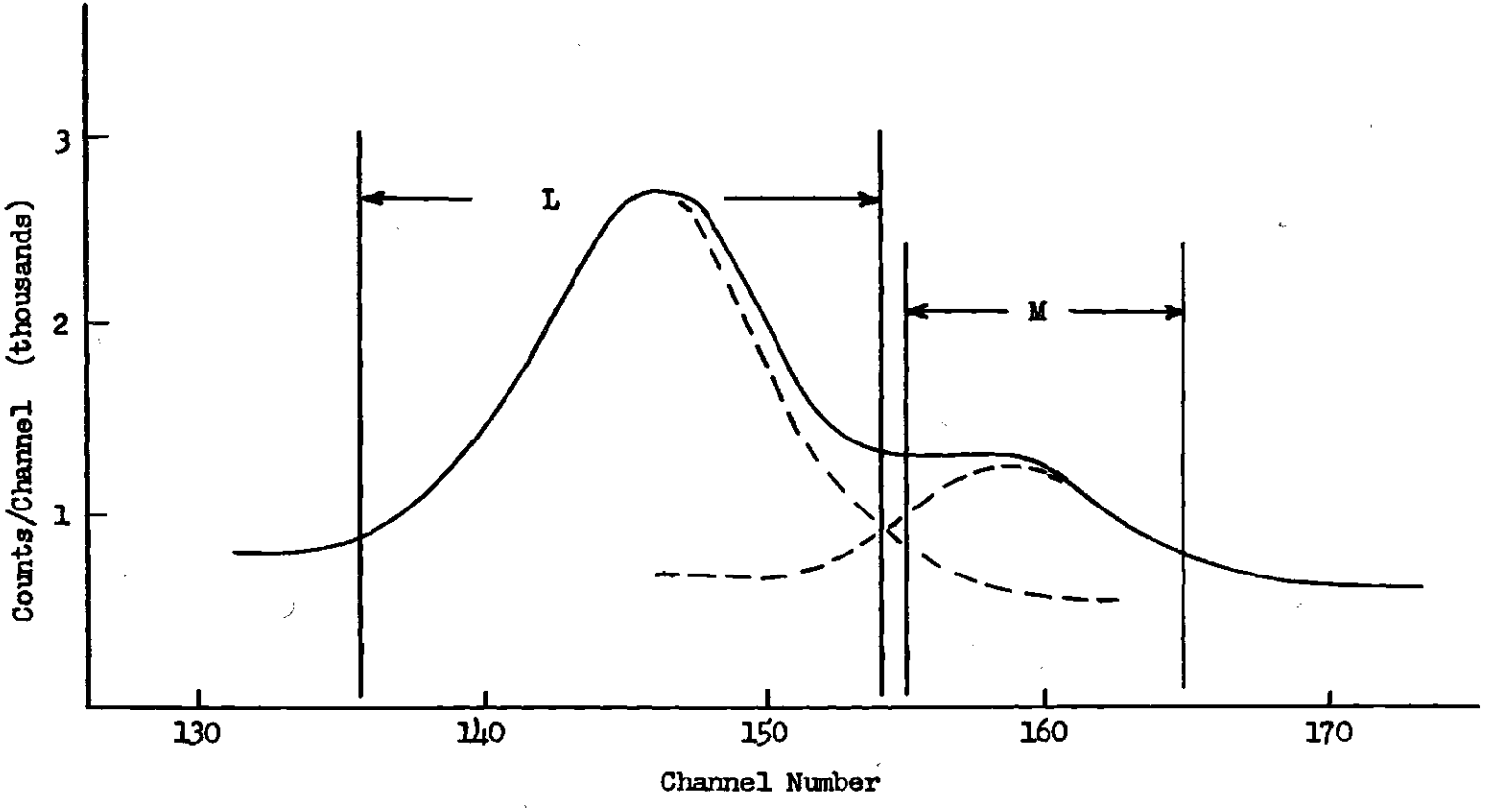

Figure 12. L and M Shell Conversion Electrons of the 570-keV Transition in Pb^{207}

Table 2. The A_2 and A_4 Coefficients for the $\gamma(1064)$-e(570) Directional Correlations in Pb^{207}

Directional Correlation	Gamma Detection Channel	Uncorrected	Solid Angle Corrected	Combined Data	Corrected for 1771-keV Compton Distribution
$\gamma(1064)$-$e_K(570)$	1	A_2 0.233(7) A_4 - 0.009(13)	0.266(11) - 0.01(2)	A_2 0.267(7) A_4 - 0.008(13)	A_2 0.281(9) A_4 - 0.010(13)
	2	A_2 0.234(5) A_4 - 0.003(10)	0.267(10) - 0.005(16)		
$\gamma(1064)$-$e_L(570)$	1	A_2 0.219(8) A_4 - 0.03(3)	0.250(11) - 0.04(3)	A_2 0.249(8) A_4 - 0.029(16)	A_2 0.262(10) A_4 - 0.032(16)
	2	A_2 0.218(7) A_4 - 0.015(12)	0.248(11) - 0.024(19)		
$\gamma(1064)$-$e_M(570)$	1	A_2 0.23(4) A_4 0.03(6)	0.26(4) 0.05(9)	A_2 0.26(3) A_4 0.06(6)	A_2 0.28(3) A_4 0.06(7)
	2	A_2 0.23(3) A_4 0.04(5)	0.27(4) 0.07(8)		

contribution of 1771 keV Compton distribution.

Directional Correlations in Cs^{133}

For directional correlation measurements in Cs^{133}, a source was constructed from a solution of $BaCl_2$ in one milliliter of HCl containing about one millicurie of Ba^{133}. This stock solution was obtained from Oak Ridge National Laboratory with a specific activity of about 1 mc/mg.

The activity was concentrated by evaporation of the stock solution to a volume of a few drops. Sources were prepared by evaporating a single drop of the concentrated solution of 1/4-mil mylar.

The conversion electron spectrum for electron energies near 320 keV was shown in Figure 9.

The gamma ray energy spectrum obtained with one of the 3X3-inch NaI(Tl) scintillation detectors is shown in Figure 13. The spectrum was recorded with a single channel pulse height analyzer using a narrow analyzer window.

The 356 keV Electron-81 keV Gamma Directional Correlation

The gamma rays selected in the single channel analyzer for the coincidence analysis are indicated in the gamma energy spectrum by the vertical lines on either side of the 81-keV gamma peak.

Although the 81-keV and 80-keV gamma rays are unresolved, it is evident from the decay scheme in Figure 3 that the 80-keV transition is not coincident with the 356-keV transition. The spectrum of conversion electrons, with kinetic energies near 320 keV, coincident with gamma rays selected by the single channel analyzer are shown in Figure 14.

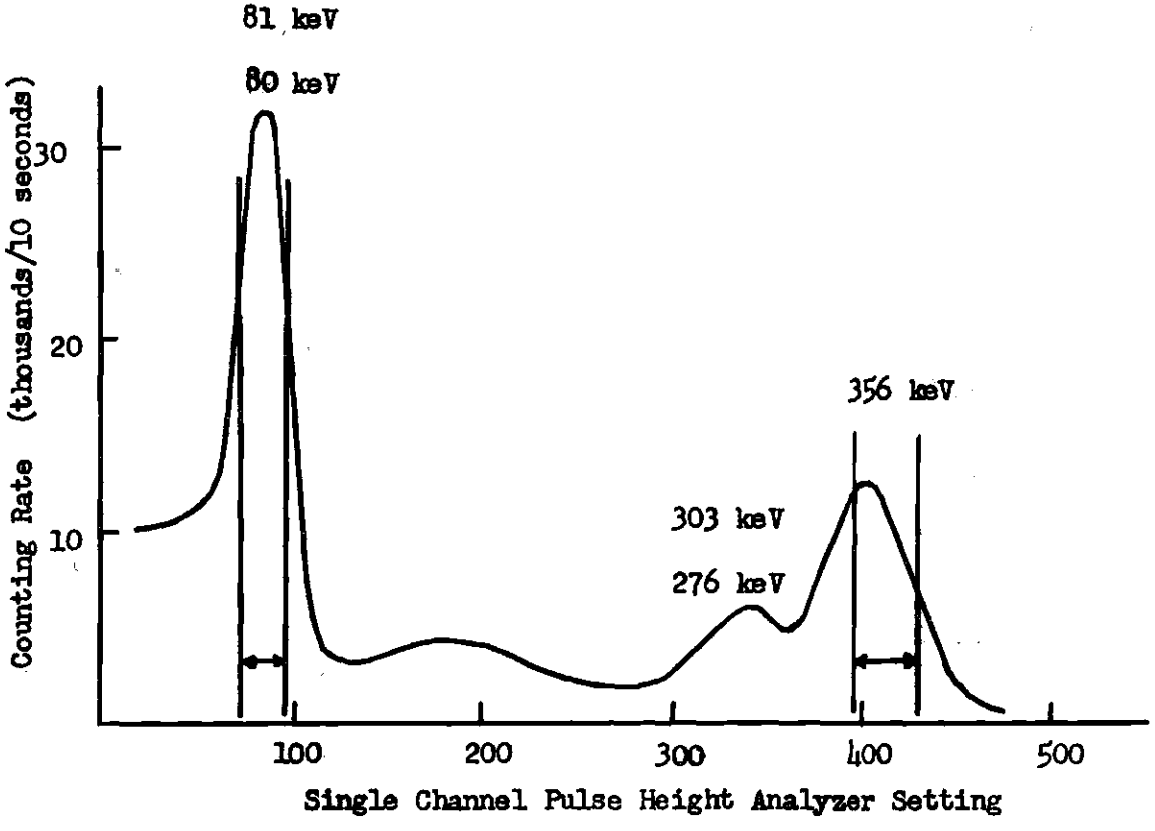

Figure 13. Cs^{133} Gamma Ray Spectrum

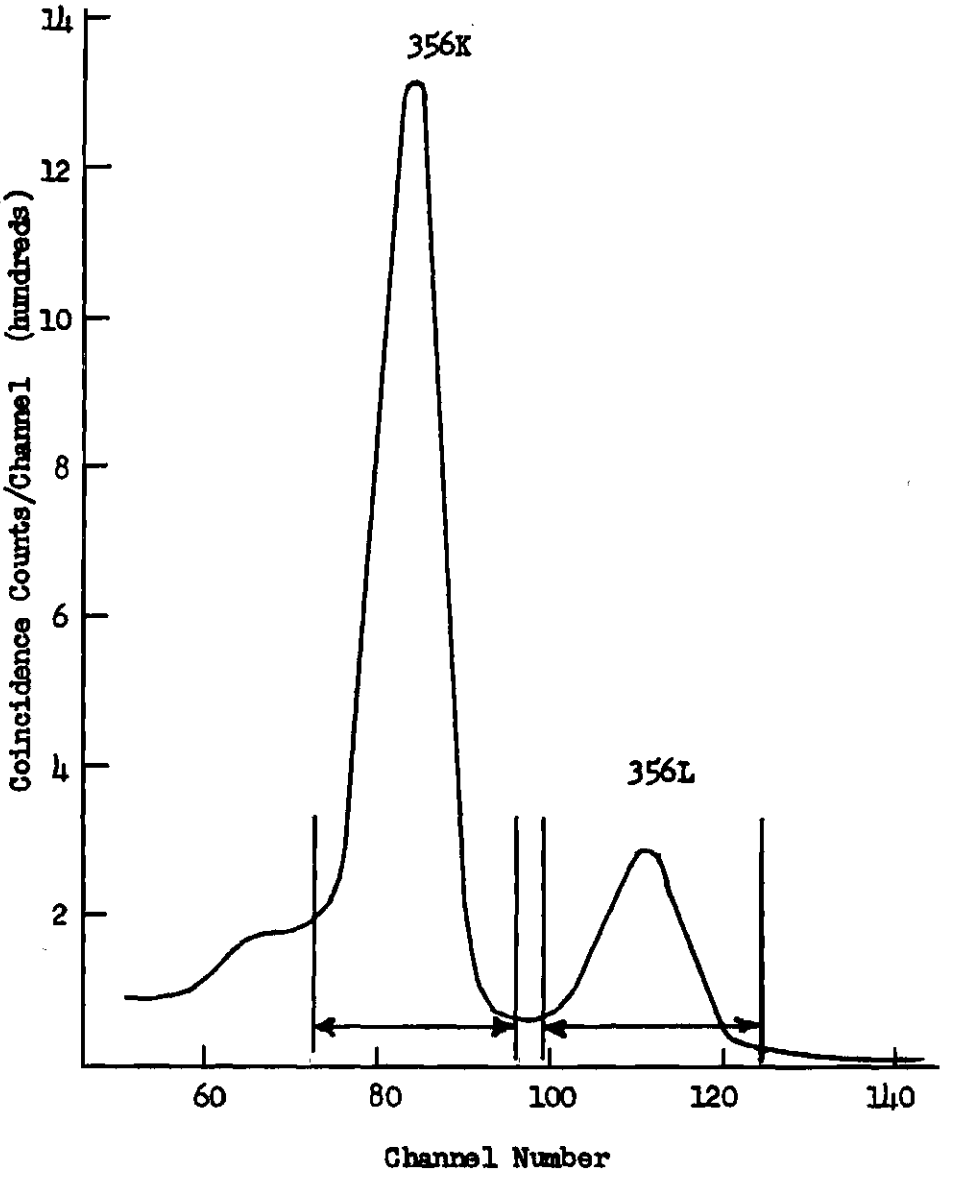

Figure 14. Conversion Electrons of the 356-keV Transition Coincident with 81-keV Gamma Rays

The K-conversion electrons of the 380-keV transition, which are unresolved from L electrons of the 356-keV transition in the electron energy spectrum in Figure 9, have been eliminated in the coincidence analysis.

The coincidence channel groups selected for the evaluation of the electron-gamma directional correlation coefficients are indicated in Figure 14. The A_2 and A_4 coefficients which were determined from coincidences in the channels denoted "356L" included coincidences involving electrons converted from M and higher shells.

Coincidence spectra were accumulated in the memory of the 400-channel analyzer for 90 minute counting intervals. Over a five week period $2X10^5$ and $5X10^4$ total (real plus accidental) coincidences were recorded in the K and L channel groups respectively. The real to accidental ratios for the two groups were 13 to 1 and 7 to 1 respectively.

The A_2 and A_4 coefficients for the K and L+M directional correlations are listed in Table 3. The coefficients listed in the column labeled "combined data" were obtained by weighting the two values obtained in separate gamma channels inversely as the square of their probable errors.

The 356 keV Gamma- 81 keV Gamma Directional Correlation

Due to the relatively long half life of the intermediate state of the cascade attenuation of the directional correlation by crystalline fields would seem likely, but none has been observed. The failure to observe attenuation of the gamma-gamma directional correlation by static quadrupole interactions has been attributed by Clikeman *et al.* (45) to the extremely small electric quadrupole moment of the Cs^{133}

Table 3. The A_2 and A_4 Coefficients for the e(356)-γ(81) Directional Correlation in Cs^{133}

Directional Correlation	Gamma Detection Channel	Uncorrected	Solid Angle Corrected	Combined Data
$e_K(356)$-γ(81)	1	A_2 0.051(5)	0.060(6)	
		A_4 0.002(9)	0.004(15)	A_2 0.056(5)
	2	A_2 0.043(5)	0.051(6)	A_4 0.000(11)
		A_4 - 0.003(9)	- 0.005(16)	
$e_{L+M}(356)$-γ(81)	1	A_2 0.045(8)	0.053(10)	
		A_4 - 0.006(14)	- 0.01(2)	A_2 0.050(8)
	2	A_2 0.038(9)	0.045(11)	A_4 - 0.000(11)
		A_4 0.000(16)	0.00(3)	

nucleus (66), (67). By measuring the gamma-gamma directional correlation using the same source employed for the electron-gamma correlation, the attenuation, if present, is the same for both measurements, and the effect on the electron particle parameter is eliminated.

Two independent measurements of the gamma-gamma directional correlation were carried out using gamma ray scintillation detectors. In the first measurement, 3X3-inch NaI(Tl) crystals were employed for the detection of both the 356-keV and 81-keV gamma rays. In the second measurement the counter used for detection of the 81-keV gamma ray was replaced by a scintillation detector consisting of a 1½-inch diameter by 3/4-inch thick NaI(Tl) crystal optically coupled to an RCA Type 6655-A photomultiplier tube. The smaller crystal was used in hopes of increasing the real to accidental ratio by reducing the number of higher energy gamma rays absorbed, hence reducing the background underlying the 81-keV peak which results from the Compton distributions of higher energy gamma rays. No significant difference was found in the results of the two measurements. The real to accidental ratio for both measurements was about 11 to 1.

The arrangement of the spectrometer electronics was modified slightly and the 400-channel analyzer was not employed in these measurements. Single channel pulse height analyzers were utilized for the selection of both gamma rays of the cascade. Triple-coincidence signals from fast-slow coincidence circuits were registered in scalers and printed on paper tape along with gamma signals from the single channel analyzers.

In Figure 13 the gamma rays of the 356-keV transition selected in the single channel analyzer are indicated by vertical lines on either side of the 356-keV peak. The 356-keV and 303-keV transitions are not completely resolved. Therefore the window of the analyzer was positioned, as indicated in the figure, on the high energy side of the 356-keV peak to exclude gamma rays of the 303-keV transition.

Coincidences between gamma rays of the 356-keV and 81-keV transitions were recorded with the axes of the gamma detectors at 90, 135, 180, 225 and 270 degrees. For each independent measurements of the directional correlation, $9X10^4$ total coincidences were recorded for each independent counting geometry in 26 five-minute counting intervals.

The data were corrected for accidental coincidences and solid angle attenuation by the gamma detector. The solid angle corrections are described in Appendix C. The A_2 and A_4 coefficients obtained from the data are listed in Table 4, and were obtained by the procedure described in Appendix B.

Table 4. The A_2 and A_4 Coefficients for the $\gamma(356)$-$\gamma(81)$ Directional Correlation in Cs^{133}.

Directional Correlation	81 keV Gamma Detector Crystal Size	Uncorrected	Solid Angle Corrected	Combined Data
$\gamma(356)$-$\gamma(81)$	1-1/2X3/4 in.	A_2 0.033(5) A_4 - 0.001(8)	0.039(5) - 0.002(13)	A_2 0.039(4) A_4 - 0.006(10)
	3X3 in.	A_2 0.032(6) A_4 - 0.005(6)	0.040(5) - 0.012(14)	

CHAPTER IV

CONVERSION ELECTRON PARTICLE PARAMETERS

Experimental electron particle parameters were obtained from the defining equation,

$$b_2 = A_2(e\gamma)/A_2(\gamma\gamma) \quad , \qquad \text{(IV-1)}$$

using measured $A_2(e\gamma)$ and $A_2(\gamma\gamma)$ coefficients.

These experimental particle parameters are compared with theoretical particle parameters obtained from the available tables of theoretical values (13), (27), (29), (30) or from individually calculated parameters (31), (43).

A ratio of the K and L shell particle parameters obtained from measurements on the same source is less sensitive to the attenuating effects of electron scattering than the individually measured parameters. Therefore, in comparing the theoretical and experimental particle parameters, it is useful to express the measured and computed parameters in the form of a ratio, $b_2(K)/b_2(L)$.

Particle Parameters for the 1064-keV and 570-keV Transitions in Pb^{207}

The experimental particle parameters for Pb^{207} are listed in Table 5 along with the A_2 coefficients from which they were determined. The $A_2(e\gamma)$ and $A_2(\gamma e)$ coefficients are taken from Tables 1 and 2. The gamma-gamma directional correlation of the 1064 keV-570 keV cascade was

Table 5. Conversion Electron Particle Parameters in Pb^{207}

Directional Correlation	A_2		b_2	Experiment	Theory	$\frac{b_2(\text{experiment})}{b_2(\text{theory})}$	Particle Parameter Ratios		
*$\gamma(1064)$-$\gamma(570)$	$A_2(\gamma\gamma)$	0.231(4)						Experiment	Theory
	$A_2(e_K\gamma)$	0.231(6)	$b_2(1064K)$	1.00(3)	1.049	0.95(3)	$\frac{b_2(1064K)}{b_2(1064L)}$	0.94(6)	1.020
$e(1064)$-$\gamma(570)$	$A_2(e_L\gamma)$	0.246(14)	$b_2(1064L)$	1.06(6)	1.028	1.04(6)	$\frac{b_2(1064L)}{b_2(1064M)}$	1.08(11)	
	$A_2(e_M\gamma)$	0.227(20)	$b_2(1064M)$	0.98(9)					
	$A_2(\gamma e_K)$	0.281(9)	$b_2(570K)$	1.22(4)	1.204	1.01(3)	$\frac{b_2(570K)}{b_2(570L)}$	1.07(6)	1.102
$\gamma(1064)$-$e(570)$	$A_2(\gamma e_L)$	0.263(10)	$b_2(570L)$	1.14(5)	1.093	1.04(4)	$\frac{b_2(570L)}{b_2(570M)}$	0.95(11)	
	$A_2(\gamma e_M)$	0.278(29)	$b_2(570M)$	1.20(13)					

*Gamma-Gamma Directional Correlation Coefficient from references (40), (42), and (43).

not measured in the present study. This correlation has been measured by several investigators (40), (42), (43). The mutual agreement of their results is a good indication that the correlation is unperturbed since the measurements were made with source materials in differing chemical environments. The $A_2(\gamma\gamma)$ coefficient employed in obtaining particle parameters from the present measurements of the $A_2(e\gamma)$ and $A_2(\gamma e)$ coefficients is a mean value of 0.231 ± 0.004 obtained from these references.

The theoretical K shell particle parameter listed in Table 5 for the E2 570-keV transition has been obtained by interpolation from the table computed by Biedenharn and Rose (13) using the point nucleus model. Since L subshells were unresolved in the present experiment, a theoretical total L-shell parameter,

$$b_2(L) = \frac{\sum_{i=1}^{3} \alpha_i b_2(L_i)}{\sum_{i=1}^{3} \alpha_i} \quad , \qquad \text{(IV-2)}$$

for the 570-keV transition was evaluated from individual L-subshell parameters, $b_2(L_i)$, by weighting them by the corresponding theoretical L subshell conversion coefficients. The L-subshell parameters for the 570-keV E2 transition were obtained by interpolating the tables of Listengarten (29) and Miranda (30). Conversion coefficients were obtained from the table of Sliv and Band (28). The L-shell parameter is listed in Table 5. It is in excellent agreement with the 1.095 value recently calculated for this transition by Hornshøj (31) using the point-nucleus model.

Although the L-particle parameter is somewhat high, the experimental K- and L-particle parameters for the 570-keV transition are in substantial agreement with the theoretical point-nucleus (unscreened) parameters available in the literature. Within the limits of the present experimental error the measured L parameter confirms the recent theoretical parameter calculations by Hornshøj (31) from which he concluded that the difference between finite size (screened) and point-nucleus (unscreened) L parameters for E2 transitions is almost immeasurable. From the present measurements there is no evidence of dynamic nuclear structure effects in the 570-keV (E2) transition in Pb^{207}.

The theoretical K shell particle parameter for the 1064-keV (M4) transition was obtained by interpolation from the table computed by Biedenharn and Rose (13). The L-shell parameter for this transition is the value computed by Hornshøj (31) on the basis of the point-nucleus (unscreened) model.

The experimental value of b_2(1064K) is in agreement with the experimental value of 0.99 ± 0.02 measured previously by Kleinheinz et al. (43). It is possible that the low experimental values, in relation to the theory, are the result of an attenuation of the correlation caused by the after effects of K hole formation. The ratio of K and L parameters provides a more significant comparison of theory and experiment. The error in the ratio of experimental K and L parameters for the 1064-keV (M4) transition is a conservative estimate. It is believed that this ratio is indeed less than one. As indicated in Table 5, this result would be in disagreement with the theoretical ratio obtained from the

point-nucleus (unscreened) parameters computed specifically for this transition by Hornshøj (31). If this small discrepancy can be taken seriously it could indicate either a small E5 admixture in the predominantly M4 transition or that screening and finite nuclear size corrections to the L parameters are significant in the pure M4 transition.

No theoretical particle parameters for the M shell are presently available for comparison with the measured values. An experimental value for the M shell particle parameter for the 1064-keV transition of 1.03 ± 0.008 has recently been reported by Rizvi and Sen (68). This value agrees with the 0.98 ± 0.09 value found in the present measurements.

Particle Parameters for the 356-keV Transition in Cs^{133}

The experimental particle parameters for Cs^{133} are listed in Table 6. The A_2 coefficients from which they were determined are taken from Tables 3 and 4.

The theoretical K-shell parameter was obtained from the work by Biedenharn and Rose (13), while the S-shell parameter was obtained by interpolation from tables of Listengarten (29) and Miranda (30).

Although the disagreement between the experimental and theoretical parameters may be statistical in origin, the possibility that the lower experimental values are the result of electron scattering in the source cannot be ruled out. Experimental K-shell parameter values of 1.64 ± 0.008 and 1.9 ± 0.5 have been reported by Thun (49) and Avignone (48) respectively.

The ratios of the theoretical and experimental K- and L-particle parameters are listed in Table 6. The ratio of experimental parameters

Table 6. Conversion Electron Particle Parameters in Cs^{133}

Directional Correlation	A_2		b_2 Experiment		b_2 Theory		$\frac{b_2(\text{experiment})}{b_2(\text{theory})}$
$\gamma(356)$-$\gamma(81)$	$A_2(\gamma\gamma)$	0.039(4)					
$e(356)$-$\gamma(81)$	$A_2(e_K\gamma)$	0.056(5)	$b_2(356K)$	1.42(17)	$b_2(356K)$	1.63	0.87(10)
	$A_2(e_{L+M}\gamma)$	0.050(8)	$b_2(356L+M)$	1.27(24)	$b_2(356L)$	1.41	0.90(17)

Particle Parameter Ratios			
	Experiment		Theory
$\frac{b_2(356K)}{b2(356L+M)}$	1.12(25)	$\frac{b_2(356K)}{b2(356L)}$	1.16

provides a comparison of the parameters which is less sensitive to attenuations such as electron scattering. Although the ratio of experimental K and L parameters is in agreement with the theoretical value for a pure E2 transition no significant comparison can be made due to the size of the experimental error.

CHAPTER V

RECOMMENDATIONS FOR FUTURE RESEARCH

Many of the details of the internal conversion transitions in Pb^{207} remain to be established. Rizvi et al. (68) have recently reported an experimental value for the K shell internal conversion coefficient for the 570 keV (E2) transition which is 30 per cent higher than the theoretical value. They attribute this result to nuclear structure effects in the internal conversion process of the E2 transition. The K and L shell particle parameters obtained in the present measurements for this transition are in agreement with the theoretical "structureless" parameter values. However, the $A_2(\gamma e)$ coefficients from which the parameters are obtained are somewhat larger than the theoretical values. This disagreement can be traced to a similar disagreement in the experimental value of $A_2(\gamma\gamma)$ which Körner et al. (40) have tentatively attributed to a small E5 admixture in the 1064-keV transition. The A_2 coefficients in each case have been corrected for a coincidence background due to the 1771 keV Compton distribution using Lazars' measurement of the 1771 keV gamma-570 keV gamma directional correlation. A remeasurement of this directional correlation is needed to completely eliminate the possibility that this correction is responsible for the higher A_2 values.

A remeasurement of the gamma-electron correlation for M-shell electrons of the 1064 keV-570 keV cascade would improve the precision of the $b_2(M)$ determination.

Two technical improvements in the correlation spectrometer are suggested for future conversion electron directional correlation studies. Directional correlations involving electrons converted from different atomic shells depend critically on the energy resolution of the electron detection system. The resolution of the lithium drift detector could be improved by reducing the stray capacitance of the electrical leads between the detector and its preamplifier. This could be accomplished through the use of a field-effect-transistor preamplifier with its first stage located inside the vacuum chamber with the detector. An alternate approach would be the redesign of the vacuum chamber to reduce the length of the electrical leads while retaining the present preamplifier.

Secondly, the data recording process should be automated to allow continuous operation of the experiment.

APPENDIX A

THEORETICAL REVIEW

This appendix is an outline of theoretical results appearing in the literature which are pertinent to the present experiments. For more comprehensive discussions of the general theory of directional correlations of nuclear radiations and the theory of conversion electron particle parameters, the reader is referred to the articles by H. Frauenfelder and R. M. Steffen (2) and M. E. Rose (1).

Directional Correlation Theory

To develop the directional correlation function $W(\theta)$ introduced in Chapter I in Equation (I-2), consider the successive emission of two nuclear particles in directions defined by the propagation vectors $\vec{k}_1$ and $\vec{k}_2$ respectively. These particles are emitted during two successive transitions of the nucleus between states characterized by their total angular momentum quantum numbers, $j_1 \rightarrow j_2$, $j_2 \rightarrow j_3$. Each nuclear state, $|j)$, is degenerate with respect to the magnetic quantum number m and consists of a set of $(2j + 1)$ substates $|jm)$.

The directional correlation function,

$$W(\theta) = W(\vec{k}_1 \cdot \vec{k}_2) \ , \qquad \text{(A-1)}$$

is defined as the relative probability that two nuclear radiations will be emitted with angle θ between their propagation vectors.

Hamilton (4) derived $W(\theta)$ for directional correlations between two gamma rays by applying second order time dependent perturbation theory to an initial system of excited nucleus and quantized radiation field. His derivation is easily generalized to apply to correlations involving emission of other types of nuclear particles. The general form for $W(\theta)$ is given by the expression

$$W(\theta) = S_1 S_2 \sum_{m_1 m_3} \left[\sum_{m_2} (j_1 m_1 | H'(\vec{k}_1) | j_2 m_2)(j_2 m_2 | H(\vec{k}_2) | j_3 m_3) \right]^2 , \quad \text{(A-2)}$$

where $H'(\vec{k}_1)$ is the interaction Hamiltonian for emission of the first particle in the direction $\vec{k}_1$ and a similar definition applies to $H(\vec{k}_2)$. Only the direction of propagation of the particles is observed and the sums S_1 and S_2 are over all non-observed quantities, such as spin orientations.

The matrix elements $(j' m' | H | j\ m)$ are probability amplitudes for the various possible transitions between m-degenerate substates.

Equation (A-2) can be simplified by choosing the quantization axis along the direction of propagation of either the first or second radiation. For definiteness, let it be chosen along the direction of the first radiation. The correlation function then becomes

$$W(\theta) = \sum_{m_2} \left\{ \sum_{m_1} \left[S_1 | (j_1 m_1 | H_1(\theta) | j_2 m_2) |^2 \right] \times \sum_{m_3} \left[S_2 (j_2 m_2 | H_2(\theta) | j_3 m_3) |^2 \right] \right\}. \quad \text{(A-3)}$$

The summands in the above equation have a particularly simple physical interpretation. The expression

$$S_1 |(j_1 m_1 | H_1(0) | j_2 m_2)|^2 = P_{m_1 m_2}(0) \qquad \text{(A-4)}$$

is the relative probability for the emission of the first radiation along the direction $\theta = 0$, during the nuclear transition $m_1 \rightarrow m_2$. Similarly

$$S_2 |(j_2 m_2 | H_2(\theta) | j_3 m_3|^2 = P_{m_2 m_3}(\theta) \qquad \text{(A-5)}$$

is the probability that the second radiation will be admitted at an angle θ during the transition $m_2 \rightarrow m_3$.

The correlation function can then be written as

$$W(\theta) = \sum_{m_1 m_2 m_3} P_{m_1 m_2}(0) P_{m_2 m_3}(\theta) \quad . \qquad \text{(A-6)}$$

Angular Distribution Functions

In order to exhibit the general angular dependence of $P_{m_2 m_3}$, several simplifying manipulations can be carried out.

The interaction Hamiltonian, $H_2(\theta)$, appearing in the transition probability $P_{m_2 m_3}$ should correspond to the emission of a particle with total angular momentum L with z-component M. The Hamiltonian is assumed to be invariant under any rotation of space coordinates and is written as an inner product of two spherical tensors of order L (69),

$$H_2 = \sum_{M=-L}^{L} H_L^M(\vec{v}_i,\vec{x}_i) = \sum_M (-1)^M A_L^{-M}(\vec{v}_i) T_L^M(\vec{x}_i) \quad . \qquad \text{(A-7)}$$

The tensor T_L^M depends only on nucleonic operators $\vec{x}_i$, while A_L^M depends only on the vectors, $\vec{v}_i$, associated with the description of the emitted particles.

These tensors are of the general form

$$A_L^M(\vec{v}_i) = a_L(v_i) Y_L^M(\theta\varphi) \quad . \qquad \text{(A-8)}$$

For gamma ray emission, for example, T_L^M would consist of multipole moments derived from nuclear charge and current densities and A_L^M would be obtained from the vector spherical harmonic expansion of the plane wave (69).

The matrix elements in $P_{m_2 m_3}$ are

$$(j_2 m_2 | H_L^M | j_3 m_3) = (-)^M A_L^{-M} (j_2 m_2 | T_L^M | j_3 m_3) \quad . \qquad \text{(A-9)}$$

The factor A_L^M can be removed from the nuclear matrix element since it is independent of the nuclear coordinates.

Since angular momentum is conserved during the transition the nuclear matrix element $(j_2 m_2 | T_L^M | j_3 m_3)$ is zero unless $m_3 = m_2 + M$, and the sum in Equation (A-7) reduces to a single term.

Using the Wigner-Ekart theorem (69) this matrix element can be expressed as

$$(j_2 m_2 | T_L^M | j_3 m_3) = \langle j_2 m_2 LM | j_3 m_3 \rangle (j_2 \| T_L \| j_3) \quad , \qquad \text{(A-10)}$$

where $\langle j_2 m_2 LM | j_3 m_3 \rangle$ is a vector-addition coefficient containing the important geometrical dependence of the matrix element. The remaining factor is called a reduced matrix element.

Substituting Equations (A-9) and (A-10) into Equation (A-5) and dropping the reduced matrix element, which is a common factor in each component $m_2 \rightarrow m_3$ of the transition $j_2 \rightarrow j_3$, the probability has the form,

$$P_{m_2 m_3} \propto \langle j_2 m_2 LM | j_3 m_3 \rangle^2 F_L^M(\theta) \quad , \qquad \text{(A-11)}$$

where

$$F_L^M(\theta) = S_2 |A_L^M(\vec{v}_i)|^2 \quad . \qquad \text{(A-12)}$$

The angular part of this expression F_L^M is called the angular distribution function for the radiation characterized by quantum numbers L and M. The sum S_2 denotes an average over all vectors, $\vec{v}_i$, except $\vec{k}_2$ which denotes the direction of emission of the particle.

The simplest example of an angular distribution function is that for spin zero particles such as the alpha particle. Only $\vec{k}_2$, the propagation vector, is required to describe the particle and no summation S_2 is needed. Using Equation (A-8)

$$F_L^M(\theta) \propto |Y_L^M(\theta\varphi)|^2 \quad . \tag{A-13}$$

The common factor $a_L^2(k)$ has been dropped since only the angular dependence is of interest. The azimuthal angular dependence is removed in the squaring of the spherical harmonic.

For gamma radiation a sum S_2 over polarization vectors is required and the angular distribution function is (70)

$$F_L^M(\theta) = \frac{(L-M)(L+M+1)}{2L(L+1)}|Y_L^{M+1}(\theta\varphi)|^2 + \frac{(L+M)(L-M+1)}{2L(L+1)}|Y_L^{M-1}(\theta\varphi)|^2$$

$$+ \frac{M^2}{2L(L+1)}|Y_L^M(\theta\varphi)|^2 \quad . \tag{A-14}$$

For an internally converted electron in a final continuum state described by a wave function $\Psi(\vec{r},t)$, F_L^M corresponds to the radial Dirac current per unit solid angle,

$$F_L^M = -r^2(\Psi^\dagger \alpha_r \Psi) \quad . \tag{A-15}$$

This distribution function has been computed by Rose et al. (15).

The Directional Correlation Function $W(\theta)$

In developing $F_L^M(\theta)$, a number of factors appearing in the directional correlation function $W(\theta)$ have been discarded for simplicity's sake in order to exhibit its angular dependence. A rigorous but lengthy calculation can be carried out to simplify the

correlation function in Equation (A-2) using the techniques introduced in Equations (A-7) through (A-10) in developing F_L^M. The general directional correlation function can be reduced to the simple form of a finite series of Legendre polynomials (13), (69),

$$W(\theta) = \sum_{\nu \text{ even}} A_\nu P_\nu(\cos\theta) \quad . \tag{A-16}$$

The maximum value of ν is determined by the selection rule

$$0<\nu< \text{Min}(2j_2, 2L_1, 2L_2) \quad ,$$

where L_1 and L_2 are the angular momenta of the first and second radiations. Yang (71) has shown that this rule follows directly from the invariance of the correlation process under rotation and inversion.

The expansion coefficients A_ν depend on the five quantum numbers j_1, j_2, j_3, L_1, and L_2.

Gamma-Gamma Directional Correlations

For a gamma-gamma cascade of pure multipole radiations, i.e., each radiation corresponding to a single value of L, the A_ν coefficients can be written in the form (13),

$$A_\nu = F_\nu(L_1, j_1, j_2) F_\nu(L_2, j_3, j_2) \quad , \tag{A-17}$$

where

$$F_{\nu}(Ljj') = (-1)^{j-j'-1}(2j'+1)^{\frac{1}{2}}(2L+1)\langle L1L,-1|\nu 0\rangle W(j'jLL;\nu j) \quad . \quad (A\text{-}18)$$

The factor $W(j'jLL;\nu j)$ is a Racah coefficient (69) and is not to be confused with $W(\theta)$. Each F_{ν} depends on only one transition in the cascade which simplifies their explicit evaluation. Numerical tables of these coefficients have been computed by A. H. Wapstra et al. (72).

For directional correlations in which one or both of the gamma rays are mixed, i.e., the gamma ray must be described by more than one value of L, the form of the correlation function is unaltered. In addition to the previous quantum numbers, the A_{ν} coefficients for mixed transitions depend on the mixing ratios of each transition as well as the additional angular momentum quantum numbers (2).

Conversion Electron Directional Correlation Particle Parameters

The expansion coefficients for conversion electron directional correlations involving pure multipole transitions depend not only on the five angular momentum quantum numbers, j_1, j_2, j_3, L_1, and L_2; but also on the parity change and the energy of the converted transition E, and the nuclear charge, Z.

The conversion electron particle parameters, b_{ν}, were defined by Rose et al. (15) by adopting the competing gamma-gamma correlation of the cascade as the standard representation of the geometry of the correlation process. For an electron-gamma correlation, the expansion coefficient is written as

$$A_\nu(e\gamma) = b_\nu(Z,E_1,\pi_1,L_1)A_\nu(\gamma\gamma) \quad , \qquad \text{(A-19)}$$

where $\nu = 2, 4$, and $\pi_1 = e, m$ refers to the parity (electric or magnetic) of the radiation. The modification of the gamma-gamma directional correlation by the conversion process is expressed in this parameter.

For electron-electron correlations the coefficient $A_\nu(ee)$ is obtained by multiplying $A_\nu(\gamma\gamma)$ by the product $b_\nu(Z,E_1,\pi_1,L_1)b_\nu(Z,E_2,\pi_2,L_2)$.

Explicit expressions for the parameters for both pure and mixed electric and magnetic multipole transitions have been derived by Rose et al. (15), Biedenharn and Rose (13), and by Ivash (73).

The theoretical particle parameters are expressed in terms of the relativistic wave functions which describe the bound and continuum states of the electron. These wave functions are of the form

$$\Psi_\kappa = \begin{pmatrix} g_\kappa(r)\chi^\mu_\kappa \\ if_\kappa(r)\chi^\mu_{-\kappa} \end{pmatrix} , \qquad \text{(A-20)}$$

where the index κ determines both the orbital and total angular momentum of the electron (74). The radial functions for the continuum-state electron will be designated g_κ and f_κ while g_κ' and f_κ' refer to the bound state.

The particle parameters for electric conversion, $\pi = e$, of an electron in an initial K-, L_I-, or M_I-shell ($\kappa' = -1$) are (13)

$$b_\nu(e) = \frac{1+\nu(\nu+1)}{2L(L+1)-\nu(\nu+1)} \times \frac{L}{2L+1} \times \frac{|L+1 + T_e|^2}{L(L+1) + |T_e|^2} \quad , \qquad \text{(A-21)}$$

where

$$T_e = \frac{[R_\kappa(e)\exp(i\delta_\kappa)]_{\kappa=L}}{[R_\kappa(e)\exp(i\delta_\kappa)]_{\kappa=-L-1}} \quad . \qquad \text{(A-22)}$$

The functions $R_\kappa(e)$ are radial integrals of the form

$$R_\kappa(e) = (\kappa'-\kappa)\int_0^\infty h_{L-1}(g_\kappa f_{\kappa'}+f_\kappa g_{\kappa'})r^2dr$$

$$+ L\int_0^\infty [h_{L-1}(g_\kappa f_{\kappa'}-f_\kappa g_{\kappa'}) + h_L(f_\kappa f_{\kappa'}+g_\kappa g_{\kappa'})]r^2dr \quad , \qquad \text{(A-23)}$$

where δ_κ is the coulomb phase defined by Biedenharn and Rose (13), and h_L and h_{L-1} are spherical Hankel functions.

The radial wave functions appearing in Equation (A-22) denote exact solutions of the Dirac equation for electrons in the unscreened Coulomb field of a point nucleus. These solutions for bound and continuum states are discussed in detail in the book by Rose (74). The numerical tables calculated by Biedenharn and Rose (13) for K-shell particle parameters for electric and magnetic transitions are based on the evaluation of radial integrals of this type.

To incorporate the effects of screening and the static effects of finite nuclear size it is necessary to re-evaluate the radial

integrals. Abandoning the point nucleus assumption, Sliv and Band (28) obtained radial electron wave functions by numerical solution of the Dirac equation in which the nuclear charge was assumed to be uniformly distributed over a sphere of radius $R = 1.2A^{1/3} \times 10^{-13}$ centimeters, where A is the atomic number. Screening was accounted for by the method of Thomas-Fermi-Dirac (83). Numerical tables of electron particle parameters based on their results are found in references (27), (29), and (30).

APPENDIX B

ANALYSIS OF EXPERIMENTAL DATA

The expansion coefficients A_2 and A_4 were introduced in defining the directional correlation function $W(\theta)$ in Chapter I. From Equation (I-2) on page 5,

$$W(\theta) = 1 + A_2 P_2(\cos\theta) + A_4 P_4(\cos\theta) \quad .$$

The A_2 and A_4 coefficients for directional correlations in Pb^{207} and Cs^{133} were obtained from recorded coincidence data by an analysis procedure consisting of five steps. Two sample calculations are outlined to illustrate the procedure.

Table 7 contains a sample of the experimental data recorded in gamma channel number one of the spectrometer during the measurement of the 1064 keV-570 keV electron-gamma correlation in Pb^{207}.

The following notation is employed for explanation of the analysis procedure.

θ is the counting angle (see Figure 3, Chapter II).

t is the counting time in hours.

n is the single channel analyzer gamma counting rate (counts/15 min.) averaged over the counting period t.

C^K, C^L, and C^M are the number of coincidences recorded in the K, L, and M channel groups of the 400-channel analyzer. These channel groups are defined in Chapter III, Figures 7 and 11.

Table 7. Data Analysis Procedure for the e(1064)-γ(570) Directional Correlation in Pb^{207}.

Angle	Counting Time (Hours)	Average Gamma Rate X10^{-3}	Coinc. Counts			1. Normalized Coinc. Counting Rates			Angles	2. Average Normalized Counting Rates		
θ	t	n	C^K_{r+a}	C^L_{r+a}	C^M_{r+a}	N^K_{r+a}	N^L_{r+a}	N^M_{r+a}		$\bar{N}^K_{r+a}$	$\bar{N}^L_{r+a}$	$\bar{N}^M_{r+a}$
90	1	1903	2549	627	181	13393	3294	951	(90,270)	13288±37	3392±22	865±12
180	1	1915	3365	881	221	17568	4600	1154	(135,225)	15733±40	3961±24	1015±15
270	1	1888	2509	633	175	13326	3521	929	(180)	17468±42	4579±26	1092±14
135	1	1905	2981	767	159	15646	4026	835				
180	1	1908	3375	834	208	17693	4372	1090		$\bar{N}^K_a$	$\bar{N}^L_a$	$\bar{N}^M_a$
225	1	1899	3017	831	151	15928	4393	797				
90	1	1898	2507	692	151	13209	3646	796		638±3	167±1	44±1
180	1	1899	3221	832	203	16958	4380	1069				
270	1	1889	2574	653	127	13629	3458	673			3.	
135	1	1902	2923	784	163	15366	4122	857				
180	1	1908	3326	875	178	17430	4585	933		$\bar{N}^K_r$	$\bar{N}^L_r$	$\bar{N}^M_r$
225	1	1909	3076	771	162	16117	4040	849				
									(90,270)	12650±37	3224±22	822±13
			C^K_a	C^L_a	C^M_a	N^K_a	N^L_a	N^M_a	(135,225)	15135±40	3793±24	971±16
135	3	1897	1135	278	88	665	163	52	(180)	16830±42	4411±26	1092±14
90	3	1903	1087	287	67	636	167	39				
180	9.5	1919	3493	930	261	639	155	48				

4. Least Squares L-shell Coefficients

$$3a_0 + 0.7500a_2 + 0.9688a_4 = 11428\pm41$$
$$0.7500a_0 + 1.3125a_2 + 0.7110a_4 = 3747\pm28$$
$$0.9688a_0 + 0.7110a_2 + 1.3056a_4 = 4079\pm29$$

$a_0 = 3607\pm28 \quad a_2 = 78\pm4 \quad a_4 = 22\pm7$

$A_2 = 0.217\pm0.011 \quad A_4 = 0.006\pm0.018$

5. Solid Angle Correction

$$A_2(\text{Corrected}) = \frac{0.217\pm0.011}{0.878} = 0.246\pm0.014$$

$$A_4(\text{Corrected}) = \frac{0.006\pm0.018}{0.645} = 0.010\pm0.028$$

N and $\bar{N}$ denote individual and average coincidence rates normalized to the gamma counting rate and to a common counting interval.

The subscripts r, a, and r+a indicate that recorded coincidences are real, accidental, or real plus accidental coincidences.

1. The coincidences, C, were normalized to a common counting interval and to the gamma counting rate,

$$N = C/nt \quad . \tag{B-1}$$

Normalization to the gamma counting rate makes a first order correction for small drifts in the electronics and for small source centering errors.

2. An average normalized counting rate, $\bar{N}_{r+a}$, was computed from a statistical sample of approximately 30 separate measurements for each of the three independent counting geometries. The data recorded at 90 and 270 degrees were averaged together as were the 135- and 225-degree data. An average normalized accidental rate $\bar{N}_a$ was also computed. For statistical samples, such as those for the accidental coincidence rates, involving individual measurements over different counting intervals, an average value was obtained by weighting each measurement by the counting time t. The standard deviation of the mean value (standard error) was obtained from each statistical sample (75). Errors listed in Table 7 are probable statistical errors obtained from the standard error (75).

3. The average normalized real coincidence counting rate $\bar{N}_r$ was obtained for each counting geometry

$$\bar{N}_r = \bar{N}_{r+a} - \bar{N}_a \quad . \tag{B-2}$$

4. The three real coincidence counting rates were fitted to the unnormalized directional correlation function,

$$w(\theta) = \sum_k a_k P_k(\cos\theta) \quad , \tag{B-3}$$

where k = 0, 2, 4.

The method of least squares specifies that this be achieved by choosing a_o, a_2, and a_4 so that

$$\Delta = \sum_i [w(\theta_i) - N^S_r(\theta_i)]^2 \tag{B-4}$$

is a minimum, where the summation is over θ_i = 90, 135, and 180 degrees and S denotes the coincidence channel group K, L or M.

The expression is minimized by differentiating with respect to a_k leading to the normal equations of the least squares method (62),

$$\sum_\mu a_\mu \sum_i P_k(\cos\theta_i)P_\mu(\cos\theta_i) = \sum_i P_k(\cos\theta_i)N^S_r(\theta_i) \tag{B-5}$$

where k, μ = 0, 2, 4. The three simultaneous equations for S = L have been written out in detail in Table 7, along with the solutions, a_o, a_2, and a_4. Numerical values for the Legendre polynomials appearing in the equations were obtained from Jahnke and Emde (76). In the solution of the equations, the statistical errors were propagated according to the

procedure described by Parrott (75). The A_2 and A_4 coefficients were obtained directly from a_0, a_2, and a_4,

$$A_2 = a_2/a_0 \quad \text{and} \quad A_4 = a_4/a_0 \quad . \tag{B-7}$$

5. The expansion coefficients were corrected for solid angle attenuation using attenuation coefficients obtained from Appendix C,

$$A_2(\text{corrected}) = \frac{A_2(\text{uncorrected})}{Q_2(1)Q_2(2)} \quad . \tag{B-8}$$

A similar expression applies for A_4.

Table 8 contains a sample of the data recorded in the measurement of the 356 keV gamma-81 keV gamma correlation in Cs^{133} using a 1½X3/4-inch NaI(Tl) crystal to detect the 81-keV gamma ray.

The following notation is employed for explanation of the analysis.

θ is the angle between the axes of the two gamma detectors.

t is the counting time measured in units of 5 minutes.

n_1 is the 356-keV gamma counting rate (counts/5 min.).

n_2 is the 81-keV gamma counting rate (counts/5 min.).

C is the number of triple coincidences recorded from the fast-slow coincidences circuits during the counting interval t.

N and $\overline{N}$ denote individual and average normalized coincidence rates.

1. The coincidences, C, were normalized to the product of the two gamma counting rates and to a common counting interval,

Table 8. Data Analysis Procedure for the $\gamma(356)$-$\gamma(81)$ Directional Correlation in Cs^{133}.

Angle	Counting Time 5 minute intervals	356-keV Gamma Count $\times 10^{-3}$	81-keV Gamma Count $\times 10^{-2}$	Coinc. Counts	1. Normalized Coinc. Counting Rate	Angles	2. Avg. Normalized Coinc. Counting Rate
θ	t	n_1	n_2	C_{r+a}	N_{r+a}		$\bar{N}_{r+a}$
180	1	1536	5824	3030	3386	(90,270)	3453±9
135	1	1558	5862	3223	3529	(135,225)	3556±9
90	1	1591	5875	3241	3468	(180)	3609±10
180	1	1589	6410	3756	3687		
225	1	1619	6416	3809	3667		
270	1	1622	6396	3685	3553		$\bar{N}_a$
180	1	1561	6460	3697	3666		295±2
135	1	1561	6630	3685	3561		
90	1	1561	6673	3624	3479		
180	1	1592	6390	3746	3682		3.
225	1	1614	6380	3639	3534		$\bar{N}_r$
270	1	1614	6356	3656	3564	(90,270)	3158±9
				C_a	N_a	(135,225)	3241±9
180	1	1598	5968	265	278	(180)	3315±10
180	1	1560	5948	276	297		
180	1	1598	5975	287	301		

4. Least Squares Fit

$$3a_0 + 0.7500a_2 + 0.9688\,a_4 = 9714\pm16$$
$$0.7500a_0 + 1.3125a_2 + 0.7110\,a_4 = 2546\pm11$$
$$0.9688a_0 + 0.7110a_2 + 1.3056\,a_4 = 3182\pm11$$

$a_0 = 3213\pm11 \quad a_2 = 106\pm15 \quad a_4 = -\,4\pm26$

$A_2 = 0.033\pm0.005 \quad A_4 = -0.001\pm0.008$

5. Solid Angle Corrected

$$A_2(\text{Corrected}) = \frac{0.033\pm0.007}{0.855} = 0.039\pm0.008$$

$$A_4(\text{Corrected}) = \frac{-0.0014\pm0.011}{0.584} = -0.002\pm0.019$$

$$N = C/n_1 n_2 t \quad . \tag{B-9}$$

2. An average normalized counting rate, $\overline{N}_{r+a}$, was computed from a statistical sample of 26 measurements for each independent counting geometry.

The standard error was computed for each statistical sample. Errors listed in Table 8 are probable statistical errors obtained from the standard error by the procedure described by Parratt (75).

3. The average normalized real coincidence rate was obtained for each counting geometry,

$$\overline{N} = \overline{N}_{r+a} - \overline{N}_a \quad . \tag{B-10}$$

4. The real coincidence counting rates were fitted to the unnormalized directional correlation function by the method of least squares as described in the previous example.

The three simultaneous normal equations have been written in detail in Table 8, along with their solutions, a_0, a_2, and a_4.

5. The resulting A_2 and A_4 coefficients were corrected for solid angle attenuation by the radiation detectors. The attenuation coefficients were obtained from Appendix C.

APPENDIX C

FINITE SOLID ANGLE CORRECTIONS

The experimental coincidence counting rate of two radiation detectors is proportional to the directional correlation function $W(\theta)$ only in the limiting case of measurements on a point source of radiation with point detectors. In practice this requires that the dimensions of the source and those of the detectors must be small in comparison to the source-to-detector distance.

In the present experiment, all sources have been treated as point sources, and corrections have been applied for the finite cylindrical geometry of the detectors according to the procedure outlined by Rose (79).

The correlation function is expressed as

$$W(\theta) = \sum_{\nu \text{ even}} A_\nu P_\nu(\cos\theta) \quad . \tag{C-1}$$

By treating each detector individually, the effect of finite detector size can be illustrated as follows. With reference to Figure 15 the measured correlation function is an average value written as

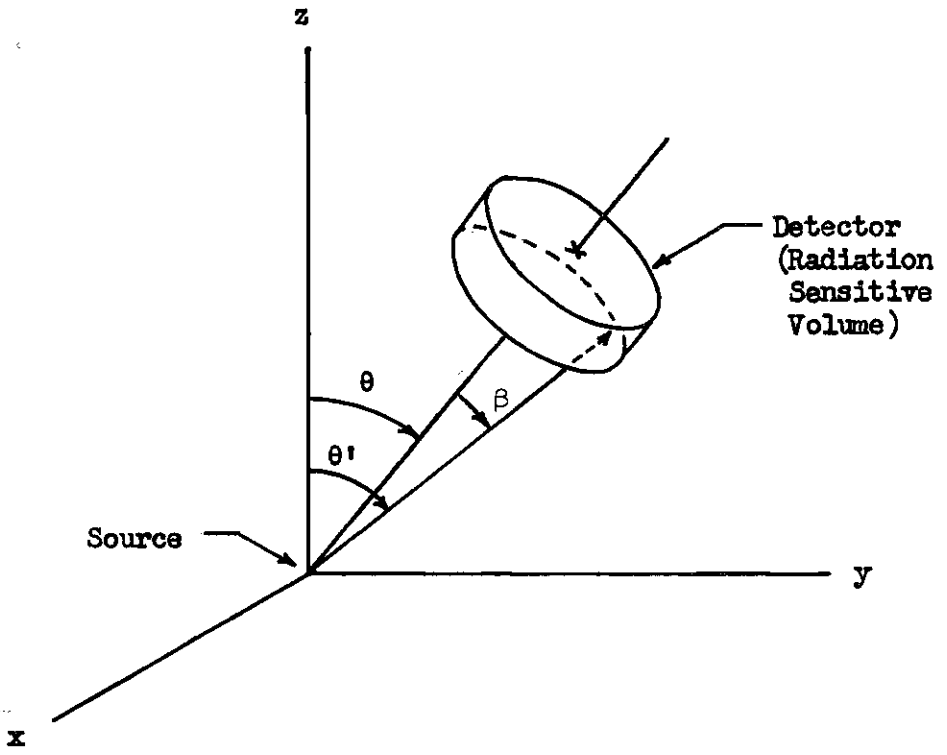

Figure 15. Counter Geometry for Solid Angle Attenuation Correction

$$\overline{W(\theta)} = \frac{\int_0^{\beta_{max}} \epsilon(E,\beta) W(\theta') d\Omega}{\int_0^{\beta_{max}} \epsilon(E,\beta) d\Omega} \qquad (C\text{-}2)$$

With the source at the origin of coordinates, the direction of emission of the radiation is defined by the angle θ' and the element of solid angle $d\Omega$. The angle θ is the angle between the coordinate z-axis and the symmetry axis of the detector. The relative efficiency, ϵ, of the detector is in general a function of the entrance angle β, and the energy of the radiation, E. The integration extends over the total solid angle subtended by the detector.

Rose has shown that, for detectors which are cylindrically symmetric about the source-detector axis, the mathematical form of the correlation function is unaffected by the finite size of the detector. However, the coefficient, A_ν, of each term in Equation (C-1) becomes multiplied by an attenuation factor Q_ν for which a simple expression can be derived. Q_ν is given by J_ν/J_0, where

$$J_\nu = \int_0^{\beta_{max}} P_\nu(\cos\beta)\,\epsilon(E,\beta)\sin\beta\, d\beta \quad . \qquad (C\text{-}3)$$

Since two radiation detectors are employed in a directional correlation measurement, A_ν must be multiplied by an attenuation factor $Q_\nu(n)$ for each detector n. The uncorrected coefficients A_ν' measured with finite-size detectors and solid angle corrected coefficients A_ν,

which would be expected from a measurement with ideal point detectors, are related by the expression

$$A_\nu'(\text{measured}) = Q_\nu(1)Q_\nu(2)A_\nu \quad . \tag{C-4}$$

For the lithium drift electron detector used in the present experiments, ϵ is approximately independent of the electron energy and the angle β. The sensitive volume of the detector shown in Figure 15 corresponds to the electron detector's two millimeter deep depletion volume. The cylindrical cross section of the radiation sensitive volume is defined by a ten millimeter diameter lucite mask described in Chapter II.

For detectors of this type, i.e., for $\epsilon = 1$, Roa (80) has evaluated the integral in Equation (C-3) directly and expressed Q_ν for $\nu = 2,4$ in terms of the fractional solid angle subtended by the detector. The results are

$$Q_2 = 1 - 3\omega + 2\omega^2 \tag{C-5}$$

and

$$Q_4 = 1 - 10\omega + 30\omega^2 - 35\omega^3 + 14\omega^4 \quad , \tag{C-6}$$

where

$$\omega = \Omega/4\pi = \sin^2(\beta_{max}/2) \quad . \qquad (C\text{-}7)$$

The solid angle, ω, is determined for each correlation measurement from a measurement, described in Chapter III, of the source-to-detector distance and from the detector mask diameter. The resulting values of $Q_2(e)$ and $Q_4(e)$ for each conversion electron correlation measurement are listed in Tables 9 and 10. Since the attenuation coefficients are independent of the kinetic energy of the electrons, they apply to directional correlations of electrons converted from all atomic shells.

For gamma scintillation detectors ϵ is the total (photopeak) absorption efficiency of the detector's cylindrical NaI(Tl) crystal. This efficiency depends on both the gamma-ray energy, E, and the angle β. The coefficients, A_2 and Q_4 have been evaluated numerically by Yates using Monte Carlo calculations (81). The gamma detector attenuation coefficients listed in Tables 9 and 10 were obtained from reference (81). For electron-gamma directional correlations the gamma detector attenuation coefficients are the same for both gamma detection channels.

Table 9. Solid Angle Attenuation Factors for the Pb^{207} Directional Correlation Measurements.

Directional Correlation	Solid Angle Attenuation Coefficients $Q_\nu(n)$, where n identifies the radiation detector				Total Solid Angle Correction Factor $Q_\nu \times Q_\nu$
e(1064)-γ(570)	Q_2(570γ)	0.908	Q_2(e)	0.971	0.882
	A_4(570γ)	0.720	Q_4(e)	0.902	0.650
γ(1064)-e(570)	Q_2(1064γ)	0.910	A_2(e)	0.963	0.876
	Q_4(1064γ)	0.713	Q_4(e)	0.877	0.626

Table 10. Solid Angle Attenuation Factors for the Cs^{133} Directional Correlation Measurements.

	Solid Angle Attenuation Coefficients $Q_\nu(n)$, where n identifies the radiation detector				Total Solid Angle Correction Factor $Q_\nu \times Q_\nu$
γ(356)-γ(81) Using a 1-1/2 X 3/4 in. Crystal for the 81-keV Gamma Detector	Q_2(356γ)	0.900	Q_2(81γ)	0.950	0.855
	Q_4(356γ)	0.695	Q_4(81γ)	0.840	0.584
γ(356)-γ(81) Using a 3 X 3 in. Crystal for the 81-keV Gamma Detector	Q_2(356γ)	0.905	Q_2(81γ)	0.875	0.792
	Q_4(356γ)	0.705	Q_4(81γ)	0.630	0.444
e(356)-γ(81)	Q_2(81γ)	0.870	Q_2(e)	0.968	0.842
	Q_4(81γ)	0.640	Q_4(e)	0.894	0.575

APPENDIX D

COINCIDENCE BACKGROUND FROM THE 1771-keV COMPTON DISTRIBUTION

In measuring the 1064 keV gamma- 570 keV electron directional correlation in Pb^{207}, gamma signals accepted in the single channel analyzers included signals resulting from Compton scattering of 1771-keV gamma rays in the detector crystal. Therefore the recorded coincidence data included an undesirable background of real coincidences between these gamma rays and electrons of the 570-keV transition. A correction for this coincidence background is described below.

The Compton distribution of the 1771-keV gamma ray has been indicated in Figure 10. The full energy peak is off the graph to the right. Figure 16 is the energy spectrum of the 1771-keV gamma ray including the full energy peak.

The expansion coefficients for the directional correlation, $W(\theta)$, obtained from the coincidence data are listed in column 3 of Table 2. The measured directional correlation function, $W(\theta)$, is a weighted sum of the 1064 keV-570 keV gamma-electron correlation function, $W_1(\theta)$, and 1771 keV-570 keV gamma-electron correlation function $W_2(\theta)$,

$$W(\theta) = \alpha W_1(\theta) + \beta(W_2(\theta) \quad , \qquad \text{(D-1)}$$

where $\alpha + \beta = 1$.

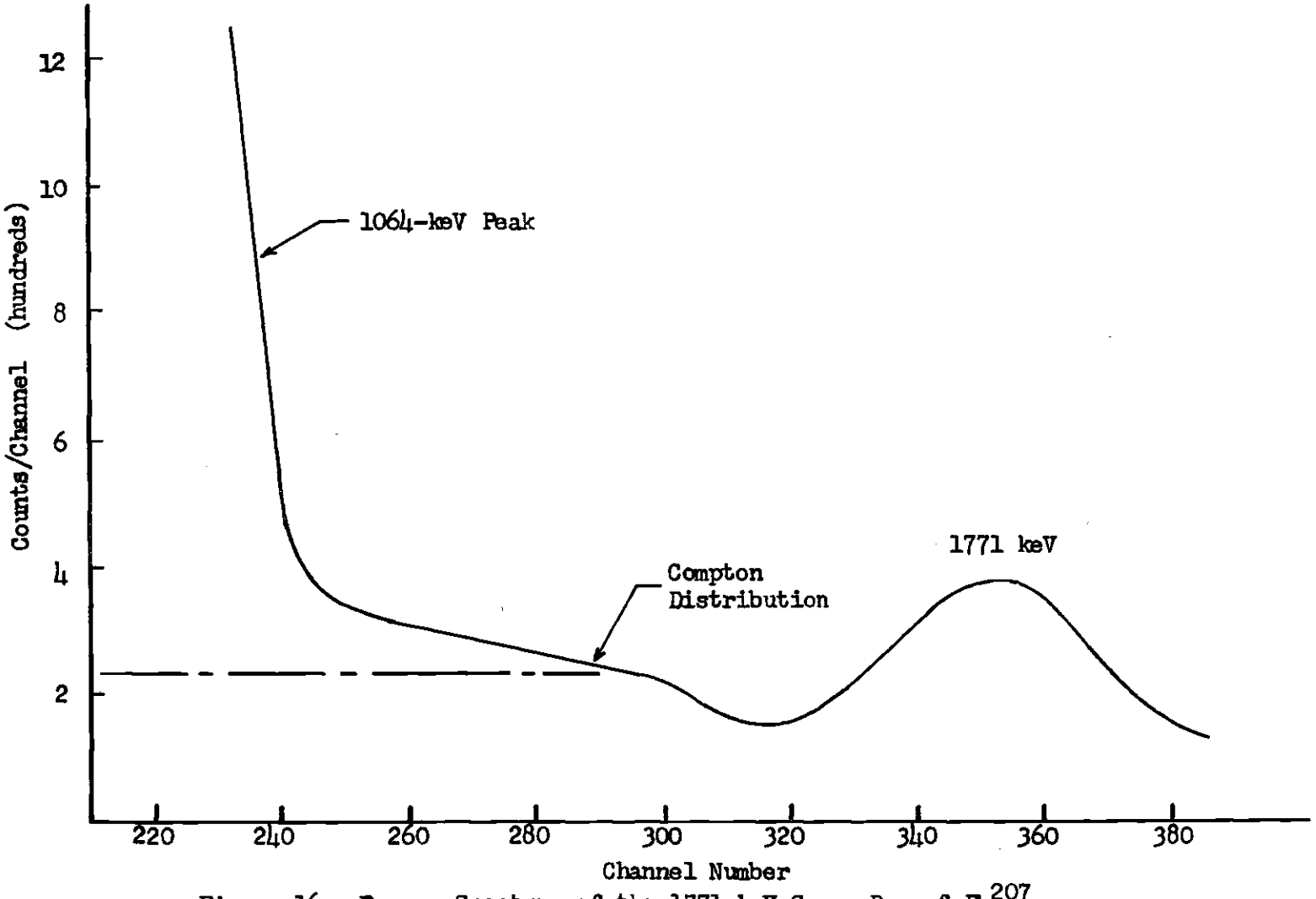

Figure 16. Energy Spectrum of the 1771-keV Gamma Ray of Pb^{207}

The weighting factors α and β are the relative number of 1064 keV and 1771 keV gamma signals with pulse heights falling within the window of the single channel analyzer. A small contribution from the 1447-keV transition has been neglected.

In Figure 10, the total number of gamma signals falling within the analyzer window is proportional to the area under the peak at 1064 keV. The analyzer window width (F.W.H.M.), which defines this area, was measured with a mercury pulser to an estimated accuracy of about 5 per cent. The area under the peak was determined to a precision of better than 1 per cent by repeated measurements with a polar planimeter.

The weighting factor is the fraction of this area resulting from the Compton distribution of the 1771-keV gamma ray. To evaluate this fraction, the Compton distribution was assumed to be constant in the neighborhood of the 1064-keV peak. The magnitude of the Compton distribution was then determined from its value on the high energy side of the 1064-keV peak in Figure 16. This value is 2.3 ± 0.3 per cent of the peak value at 1064 keV. The resulting weighting factors with their estimated errors are

$$\beta = 0.049(10) \quad \text{and} \quad \alpha = 0.951(10) \quad . \qquad \text{(D-2)}$$

These weighting factors were employed to correct A_2 and A_4 coefficients obtained from data recorded in both gamma detection channels of the spectrometer.

From Equation (D-1), the measured expansion coefficients can be

expressed as follows:

$$A_2(\text{measured}) = \alpha A_2(1064\gamma,570e) + \beta A_2(1771\gamma,570e) \quad . \qquad (D\text{-}3)$$

Using Equation (I-5),

$$A_2(1771\gamma,570e) = b_2(570e)A_2(1771\gamma,570\gamma) \quad . \qquad (D\text{-}4)$$

Using this expression in Equation (D-3) and solving for $A_2(1064\gamma,570e)$, one obtains the expression

$$A_2(1064\gamma,570e) = \frac{A_2(\text{measured})}{\alpha} - \frac{\beta b_2(570e)A_2(1771\gamma,570\gamma)}{\alpha} \quad . \qquad (D\text{-}5)$$

A similar expression applies for the A_4 coefficient,

$$A_4(1064\gamma,570e) = \frac{A_4(\text{measured})}{\alpha} - \frac{\beta b_4(570e)A_4(1771\gamma,570\gamma)}{\alpha} . \qquad (D\text{-}6)$$

In evaluating Equations (D-4) and (D-5) the coefficients of the 1771 keV gamma-570 keV gamma directional correlation measured by Lazar (78) have been employed,

$$A_2(1771\gamma,570\gamma) = 0.0087(89) \quad \text{and} \quad A_4(1771\gamma,570\gamma) = 0.029(14) \quad . \qquad (D\text{-}7)$$

The second term on the right side of Equation (D-5) contains the unknown particle parameter $b_2(570e)$. To evaluate this equation the

theoretical b_2 parameters listed in Table 5 were employed. Due to the small magnitude of the product $\beta A_2(1771\gamma,570\gamma)$ the second term in Equation (D-5) is less than 1 per cent of the first term. Therefore the uncertainty in the particle parameter b_2 appearing in the equation does not seriously affect the determination of the corrected expansion coefficients.

In applying Equation (D-6) the recurrence relationship between b_2 and b_4 has been used to obtain the theoretical b_4 parameters for K- and L-shell electrons,

$$b_4(E2) = [7/2 - (5/2)b_2(E2)] \qquad (D\text{-}8)$$

The total L-shell parameter, $b_4(L)$, obtained from Equation (D-8) is only an approximation since this equation applies only to electrons converted from the L_I and L_{II} subshells (73).

Since no theoretical M shell particle parameters are available, the correction of the $A_2(M)$ and $A_4(M)$ coefficients were made by assuming that the M shell particle parameters were equal to the L-shell parameters (77), (37).

As a sample calculation the measured $A_2(1064\gamma,570e)$ coefficient has been corrected for the 1771-keV Compton coincidence background using Equation (D-5):

$$A_2(1064\gamma, 570e) = \frac{0.2494(80)}{0.951(10)} + \frac{0.049(10) \times 1.093 \times 0.0087(89)}{0.951(10)}$$

$$= 0.2622(100) + 0.0005(5)$$

$$= 0.263(10)$$

BIBLIOGRAPHY

1. M. E. Rose, Internal Conversion Theory, in Internal Conversion Processes (ed. J. H. Hamilton): Academic Press Incorporated, New York, 1966.

2. H. Frauenfelder and R. M. Steffen, Angular Correlations, in Alpha-, Beta-, and Gamma-Ray Spectroscopy (ed. K. Siegbahn): North-Holland Publishing Company, Amsterdam, 1965.

3. H. Aeppli, A. S. Bishop, H. Frauenfelder, M. Walter and W. Zunti, Physical Review, 82 (1951) 550.

4. D. R. Hamilton, Physical Review, 58 (1940) 122.

5. E. L. Brady and M. Deutsch, Physical Review, 72 (1947) 870.

6. E. L. Brady and M. Deutsch, Physical Review, 74 (1948) 1541.

7. M. Deutsch and F. Metzger, Physical Review, 74 (1948) 1542.

8. D. S. Ling and D. L. Falkoff, Physical Review, 76 (1949) 1639.

9. J. W. Gardner, Proceedings of the Royal Society of London, A62 (1949) 763.

10. G. Racah, Physical Review, 62 (1942) 438.

11. D. L. Falkoff and G. E. Uhlenbeck, Physical Review, 79 (1950) 334.

12. J. M. Blatt and L. C. Biedenharn, Reviews of Modern Physics, 24 (1952) 258.

13. L. C. Biedenharn and M. E. Rose, Reviews of Modern Physics, 25 (1953) 729.

14. F. Coester and J. M. Jauch, Helvetica Physica Acta, 26 (1953) 3.

15. M. E. Rose, L. C. Biedenharn, and G. B. Arfken, Physical Review, 85 (1951) 5.

16. E. L. Church and J. Weneser, Annual Review of Nuclear Science, 10, (1960) 193.

17. B.-G. Pettersson, L. Holmberg, and T. R. Gerholm, Experimental Studies of Dynamic Contributions to E2 Conversion, in Internal Conversion Processes (ed. J. H. Hamilton): Academic Press Incorporated, New York, 1966.

BIBLIOGRAPHY (Continued)

18. T. A. Green and M. E. Rose, Physical Review, 110 (1958) 105.

19. S. DeBenedetti and R. W. Findley, The Coincidence Method, in Handbuch der Physik, vol. 45, Springer-Verlay, Berlin, 1958.

20. F. S. Goulding, Multi-channel Pulse-amplitude Analyzers, in Alpha-, Beta-, and Gamma-Ray Spectroscopy (ed. K. Siegbahn): North-Holland Publishing Company, Amsterdam, 1965.

21. E. M. Pell, National Academy of Science, Report NAS-NSS32, Publication 871 (1961) 136.

22. H. C. Coburn, J. V. Kane, and S. Frankel, Physical Review, 105 (1957) 1293.

23. S. Frankel, Physical Review, 83 (1951) 673.

24. B.-G. Pettersson, J. E. Thun, and T. R. Gerholm, Nuclear Physics, 24 (1961) 223.

25. N. Goldberg and S. Frankel, Physical Review, 100 (1955) 1355.

26. T. R. Gerholm and B.-G. Pettersson, Conversion Electron-Gamma Direction Correlations, in Internal Conversion Processes (ed. J. H. Hamilton): Academic Press Incorporated, New York, 1966.

27. I. M. Band, M. A. Listengarten, L. A. Sliv and J. E. Thun, Particle Parameters for Angular Correlations of Conversion Electrons, in Alpha-, Beta-, and Gamma-Ray Spectroscopy (ed. K. Siegbahn): North-Holland Publishing Company, Amsterdam, 1965.

28. I. M. Band, M. A. Listengarten and L. A. Sliv, Tables of the Conversion Matrix Elements and Phases, in Alpha-, Beta-, and Gamma-Ray Spectroscopy (ed. K. Siegbahn): North-Holland Publishing Company, Amsterdam, 1965.

29. M. A. Listengarten, I. M. Band, E. F. Zganjar, and J. H. Hamilton, L Shell Particle Parameters for Angular Correlations of Conversion Electrons, in Internal Conversion Processes (ed. J. H. Hamilton) Academic Press Incorporated, New York, 1966.

30. A. Miranda, P. Hornshøj and B. I. Deutch, L Shell Particle Parameters for Angular Correlation of Conversion Electrons, in Internal Conversion Processes (ed. J. H. Hamilton): Academic Press Incorporated, New York, 1966.

31. P. Hornshøj, B. I. Deutch and A. Miranda, Nuclear Physics, A95 (1967) 65.

BIBLIOGRAPHY (Continued)

32. I. M. Band, M. A. Listengarten, and L. A. Sliv, Tables of Conversion Matrix Elements and Phases, in Internal Conversion Processes (ed. J. H. Hamilton): Academic Press Incorporated, New York, 1966.

33. A. K. Ustinova, Journal of Experimental and Theoretical Physics (U.S.S.R.) 10 (1960) 216.

34. B. I. Deutch and P. Hornshøj, Particle Parameters Measured in Pure Transitions, in Internal Conversion Processes (ed. J. H. Hamilton): Academic Press Incorporated, New York, 1966.

35. R. B. Frankel, D. A. Shirley, and N. J. Stone, Physical Review, 136 (1964) 577.

36. B. I. Deutch and P. Hornshøj, Nuclear Physics, 53 (1964) 497.

37. W. L. Croft, J. H. Hamilton, and B.-G. Pettersson, K and L. Shell Particle Parameters of the 82.4 keV E2 Transition in Yb^{170}, in Internal Conversion Processes (ed. J. H. Hamilton): Academic Press Incorporated, New York, 1966.

38. H. M. Neumann and I. Perlman, Physical Review, 81 (1951) 958.

39. D. E. Alburger and A. W. Sunyar, Physical Review, 99 (1955) 695.

40. H. J. Körner, K. Auerbach, J. Braunsfurth, and E. Gerdau, Nuclear Physics, 86 (1966) 395.

41. F. K. McGowan and E. C. Campbell, Physical Review, 92 (1953) 523.

42. S. Gustafsson, K. Johansson, E. Karlsson, and A. G. Svensson, Physics Letters, 10 (1964) 191.

43. P. Kleinheinz, R. Vukanovic, L. Samuelsson, D. Krmpotic, H. Lindstrom and K. Siegbahn, Nuclear Physics, 93 (1967) 63.

44. F. K. McGowan, Physical Review, 92 (1953) 524.

45. E. Bodenstedt, H. J. Körner, and E. Matthias, Nuclear Physics, 11 (1959) 584.

46. L. I. Yin and M. L. Wiedenbeck, Nuclear Physics, 54 (1964) 86.

47. E. B. Nieschnidt, C. E. Mandeville, L. D. Ellsworth, and D. D. Bornemeier, Physical Review, 136 (1964) 597.

BIBLIOGRAPHY (Continued)

48. F. T. Avignone, III, C. H. Braden, E. T. Patronis, Jr., and L. D. Wyly, Nuclear Physics, 80 (1966) 314.

49. J. E. Thun, S. Fornkvist, K. Bonde Nielsen, H. Snellman, F. Falk, and A. Mocoroa, Nuclear Physics, 88 (1966) 289.

50. H. L. Hennecke, J. C. Manthuruthil, O. Bergman, and C. R. Cothern, Physical Review (to be published).

51. L. D. Hendrich and F. T. Avignone, III, Physical Review (to be published).

52. F. Brown, R. L. Graham, G. T. Ewan, and J. Uhler, Canadian Journal of Physics, 39 (1961) 779.

53. K. Siegbahn, C. Nordling, S.-E. Karlsson, S. Hagstrom, A. Fahlman, and I. Andersson, Nuclear Instruments and Methods, 27 (1964) 173.

54. F. M. Clikeman and M. G. Stewart, Physical Review, 117 (1960) 1052.

55. A. P. Arya, Physical Review, 122 (1961) 549.

56. B. N. Subba Rao, Nuclear Physics, 27 (1961) 28.

57. M. R. Meder, H. E. Williams, and F. E. Durham, Bulletin of the American Physical Society, 11 (1966) 395.

58. Y. K. Agarwal, C. V. K. Baba, and S. K. Bhattacherjee, Nuclear Physics, 58 (1964) 651.

59. K. Siegbahn, Beta-Ray Spectrometer Theory and Design, in Alpha-, Beta-, and Gamma-Ray Spectroscopy (ed. K. Siegbahn): North-Holland Publishing Company, Amsterdam, 1965.

60. A. H. Wapstra, The Coincidence Method, in Alpha-, Beta-, and Gamma-Ray Spectroscopy (ed. K. Siegbahn) North-Holland Publishing Company, Amsterdam, 1965.

61. M. E. Rose, Physical Review, 91 (1953) 610.

62. A. J. Ferguson, Angular Correlation Methods in Gamma-Ray Spectroscopy, North-Holland Publishing Company, Amsterdam, 1965.

63. S. Hagstrom, C. Nordling, and K. Siegbahn, Tables of Electron Binding Energies and Kinetic Energy Versus Magnetic Rigidity, in Alpha-, Beta-, and Gamma-Ray Spectroscopy (ed. K. Siegbahn): North-Holland Publishing Company, Amsterdam, 1965.

BIBLIOGRAPHY (Continued)

64. E. A. Leventhal, Nuclear Instruments and Methods, 35 (1965) 325.

65. G. T. Ewan and R. L. Graham, Internal Conversion Studies at Very High Resolution, in Alpha-, Beta-, and Gamma-Ray Spectroscopy (ed. K. Siegbahn): North-Holland Publishing Company, Amsterdam, 1965.

66. Von H. Bucka, H. Kopfermann, and E. W. Otten, Annalen Der Physik, 4 (1959) 39.

67. Von H. Bucka and G. von Oppen, Annalen Der Physik, 10 (1962) 119.

68. S. I. H. Rizvi and S. K. Sen, Bulletin of the American Physical Society, 12 (1967) 715.

69. M. E. Rose, Elementary Theory of Angular Momentum, John Wiley and Sons, Incorporated, New York, 1957.

70. J. D. Jackson, Classical Electrodynamics, John Wiley and Sons, Incorporated, New York, 1962.

71. C. N. Yang, Physical Review, 74 (1948) 764.

72. A. H. Wapstra, G. J. Nijgh and R. van Lieshout, Nuclear Spectroscopy Tables, North-Holland Publishing Company, Amsterdam, 1959.

73. E. V. Ivash, Nuovo Cimento, 9 (1958) 136.

74. M. E. Rose, Relativistic Electron Theory, John Wiley and Sons, Incorporated, New York, 1961.

75. L. G. Parratt, Probability and Experimental Errors in Science, John Wiley and Sons, Incorporated, New York, 1961.

76. E. Jahnke and F. Emde, Tables of Functions, With Formulae and Curves, Dover Publications, New York, 1945.

77. T. Yamazaki, Angular Correlations Involving Conversion Electrons, in Internal Conversion Processes (ed. J. H. Hamilton): Academic Press Incorporated, New York, 1966.

78. N. H. Lasar and E. D. Klema, Physical Review, 98 (1955) 710.

79. M. E. Rose, Physical Review, 91 (1953) 610.

80. B. N. S. Roa, Nuclear Instruments and Methods, 36 (1965) 59.

BIBLIOGRAPHY (Concluded)

81. M. J. L. Yates, Finite Solid Angle Corrections, in Alpha-, Beta-, and Gamma-Ray Spectroscopy (ed. K. Siegbahn): North-Holland Publishing Company, Amsterdam, 1965.

82. D. L. Falkoff and G. E. Uhlenbeck, Physical Review, 79 (1950) 323.

83. L. I. Shiff, Quantum Mechanics, McGraw-Hill Book Company Incorporated, New York, 1955.

VITA

Russell McDill Brengelman was born in Gadsden, Alabama, on June 15, 1939. Following his graduation from Gadsden High School in 1958 he entered Auburn University in Auburn, Alabama. He was elected to membership in Sigma Pi Sigma, Tau Beta Pi, and Pi Mu Epsilon. He graduated with the degree of Bachelor of Engineering Physics in June of 1962. He began graduate study in physics at Georgia Institute of Technology in 1962 and received the M.S. degree two years later. During his graduate study he has held both research and teaching assistantships in the School of Physics. He is a member of Sigma Xi and the American Physical Society. He married Elizabeth Ruth McMahon of Atlanta, Georgia, in 1964, and they have one son, Mark Russell.